Yohkoh Analysis Guide
Instrument Manual

Ver 1.06 Ed: M.D. Morrison 6-Nov-92
Ver 2.00 Ed: M.D. Morrison 25-Jan-94
Ver 2.91 Ed: R.D. Bentley 4-Oct-2004
Ver 2.92 Ed: A. Takeda(Yohkoh Legacy data Archive) date below

This Copy Produced: March 25, 2014

Prepared at
Mullard Space Science Laboratory
University College London

Contents

1 Introduction to the Yohkoh Instruments **1**
1.1 Yohkoh Observing Modes . . . 1
1.2 Bragg Crystal Spectrometer (BCS) . . . 1
1.2.1 Instrument Modes . . . 1
1.3 Hard X-Ray Telescope (HXT) . . . 1
1.4 Soft X-Ray Telescope (SXT) . . . 1
1.4.1 Sequence Tables . . . 2
1.4.2 Automatic Exposure Control (AEC) . . . 3
1.4.3 Automatic Region Selection (ARS) . . . 3
1.5 Wide Band Spectrometer (WBS) . . . 4
1.6 Spacecraft Attitude Control System (ACS) . . . 5

2 Bragg Crystal Spectrometer (BCS) **6**
2.1 Instrument Characteristics . . . 6
2.1.1 Wavelength Range . . . 6
2.1.2 Data Compression . . . 6
2.2 Instrument Calibration . . . 7
2.2.1 Sensitivity Functions . . . 7
2.2.2 Wavelength Resolution . . . 8
2.3 Detector Performance . . . 8
2.3.1 Detector Gain and Energy Resolution . . . 8
2.3.2 Position Resolution . . . 8
2.3.3 Digitization Spikes . . . 9
2.4 Detector Background . . . 9
2.4.1 Energy Discrimination . . . 9
2.4.2 Particle Background . . . 9
2.4.3 Germanium Fluorescence . . . 9
2.4.4 Effect of Gain Depression . . . 9
2.5 Dynamic Range and Count Rate Effects . . . 10
2.5.1 Deadtime Correction . . . 10
2.5.2 Saturation . . . 10
2.5.3 Gain Depression . . . 11
2.5.4 Rate-dependent Distortion . . . 11
2.6 Data Features . . . 11
2.6.1 Queued Data . . . 11
2.6.2 Timing of Spectra . . . 11
2.6.3 Last Spectral Bin . . . 12
2.6.4 Medium-rate Spectral Data in Autumn 1991 . . . 12
2.6.5 Single Event Upsets . . . 12
2.7 Contact Persons . . . 12
2.8 References . . . 12

3 Hard X-Ray Telescope (HXT) **13**
3.1 Overview . . . 13
3.2 General information . . . 13
3.2.1 Observations with HXT . . . 13

3.2.2 Detector gain calibration . . . 13
3.2.3 Background counts . . . 14
3.3 Some detailed information . . . 14
3.3.1 Modulation patterns . . . 14
3.3.2 Spectral Energy Response . . . 15
3.3.3 Pre-storage of HXT data in DP . . . 15
3.3.4 Data compression . . . 15
3.4 Contact Persons . . . 16
3.5 References . . . 16

4 Soft X-Ray Telescope (SXT) 17
4.1 Overall Response Function for SXT . . . 17
4.1.1 CCD Camera Signal . . . 17
4.1.2 SXT Effective Area . . . 21
4.1.3 Reading the SXT Effective Area File . . . 22
4.1.4 SXT Response to Thermal Plasma . . . 22
4.1.5 Reading the SXT Response Function File . . . 23
4.1.6 Relative Alignment of X-Ray and Optical Images . . . 24
4.2 The CCD Camera . . . 25
4.2.1 Saturation Effects . . . 25
4.2.2 Effect of CCD Contamination . . . 25
4.2.3 SXT Images Taken with the CCD Warm . . . 26
4.2.4 Artifacts in Optical Images from Radiation Damage . . . 26
4.2.5 SAA Effects on Images . . . 26
4.2.6 Subtleties of Background Subtraction . . . 26
4.2.7 Charge Bleed-back . . . 27
4.2.8 CCD Pixelization . . . 27
4.2.9 What is Really Zero Signal Level in Data Numbers (DN)? . . . 27
4.3 The Mirror, Lens or Filters . . . 28
4.3.1 Scattering by ND X-ray Filter . . . 28
4.3.2 Point Spread Function . . . 28
4.3.3 Mirror Scatter . . . 28
4.3.4 Vignetting Correction . . . 29
4.3.5 Stray Visible Light . . . 30
4.4 Other Instrument and Operations Features . . . 31
4.4.1 Data Compression . . . 31
4.4.2 Use of Low-8 Images in Optical Data . . . 31
4.4.3 Filter Alternation During AEC . . . 32
4.4.4 The Roll Angle in the SXT Images . . . 32
4.4.5 Incorrect Location of Image Pieces in Some PFIs . . . 32
4.4.6 Preparation of SFD images . . . 33
4.5 Contact Persons . . . 33
4.6 References . . . 33

5 Wide Band Spectrometer (WBS) 34
5.1 Basic Instrument Characteristics . . . 34
5.2 Soft X-Ray Spectrometer (SXS) . . . 34
5.3 Hard X-Ray Spectrometer (HXS) . . . 35
5.4 Gamma-Ray Spectrometer (GRS) . . . 35
5.5 WBS Output Data . . . 36
5.6 Contact Persons . . . 37
5.7 References . . . 38

6 Spacecraft Attitude, Ephemeris and Coordinate Systems 39
6.1 Spacecraft Attitude Control System (ACS) . . . 39
6.1.1 Inertial Reference Unit (IRU) . . . 39
6.1.2 Two-dimensional Fine Sun Sensor (TFSS) . . . 39
6.1.3 Star Tracker (STT) . . . 39
6.1.4 Geomagnetic Sensors (GAS) . . . 39
6.1.5 HXT Aspect Sensor (HXA) . . . 39
6.1.6 Attitude Determination Software (ADS) . . . 39
6.2 ACS Performance . . . 39
6.2.1 Pointing Accuracy . . . 39
6.2.2 Spacecraft Jitter . . . 39
6.2.3 Sensor Problems . . . 40
6.3 Instrument and Spacecraft Co-alignment . . . 40
6.4 Spacecraft Ephemeris . . . 40
6.5 Contact Persons . . . 40
6.6 References . . . 40

A Details on the Time Tags on the Data 41
A.1 Bragg Crystal Spectrometer (BCS) . . . 41
A.2 Hard X-Ray Telescope (HXT) . . . 41
A.3 Soft X-Ray Telescope (SXT) . . . 42
A.4 Wide Band Spectrometer (WBS) . . . 43

B Details of the SXT CCD Pixels 45

C Dates of Significant SXT Activities 46
C.1 Dates that SXT CCD was Baked Out . . . 46
C.2 Table of Number of SXT Images and Dark Current Levels . . . 47
C.3 Dates of SXT Entrance Filter Failures . . . 49

D Attitude Control System (ACS) Related Items 50
D.1 Dates When Yohkoh was at non-zero Roll . . . 50

E Miscellaneous Yohkoh Information 51
E.1 Amount of Yohkoh Data per Week . . . 51

F Web Version of the YAG 54

List of Figures

2.1 The BCS data compression algorithm 7
4.2 Factors that determine the SXT effective area. Panel (a) shows the double entrance filter transmission; panel (b) shows the mirror reflectivity including the obscuration from the support structures; panel (c) shows the CCD quantum efficiency. Panel (d) is the product of panels (a), (b), and (c). 18
4.3 The effective area of the SXT: The thick curve shows gives the effective area for the indicated filter. The thin curve is the open filter case (no analysis filter) effective area over-plotted for comparison. 19
4.4 The total SXT signal as a function of $\log_{10}(T_e)$ for the open filter and the analysis filters as indicated. NOTE: Be and Al12 are mistakenly reversed in Tsuneta *et al.*, (1991). 20
4.5 Ratios of the SXT response functions. For the curve marked "Be119/(2×Al12)" the effective observing time with the Al12 filter has been doubled with respect to the Be119 filter. For the curve marked "2×Al12/Al.1" the effective observing time with the Al12 filter has again been doubled, this time with respect to the Al.1 filter. 21
4.6 Relative alignment of the X-ray and optical images (as of 1992 analysis). According to the final calibration in 2008, the NB and WB boresights are both in the NE of the X-ray boresight. 24
4.7 The effective area (or vignette function) as a function of off-axis angle. The solid curve was derived from C K and Al K data and the dashed curve from Ag L data. 30
A.8 Timing of HXT data for Hi/Hi telemetry frames 41
A.9 Timing of HXT data for Med/Med telemetry frames 41
A.10 Timing of HXT data for Hi/Med telemetry frames 42
A.11 Timing of HXT data for Med/Hi telemetry frames 42
A.12 Timing of SXT data 43
A.13 Timing of WBS SXS-PH data 43
A.14 Timing of WBS HXS-PH data 44
A.15 Timing of WBS GRS-PHL data 44
A.16 Timing of WBS SXS-PC data 44
B.17 SXT CCD Pixel Layout 46

1 Introduction to the Yohkoh Instruments

1.1 Yohkoh Observing Modes

There are generally two Data Processor (DP) modes when Yohkoh is taking scientific data, FLARE mode and QUIET mode. Yohkoh uses the WBS HXS and SXS instruments to monitor solar activity and when a threshold is passed the spacecraft (S/C) enters FLARE mode. There are times when Yohkoh is in FLARE mode but there is no flare.

There are three different telemetry rates, but only two are used when observing the sun. HIGH rate is 32 Kbits/s (a major frame every 2 s) and MEDIUM is 4 Kbits/s (a major frame every 16 s). When first entering FLARE mode, the DP goes into HIGH rate. After 10 minutes, it will go into MEDIUM rate if the intensity of the flare has subsided, but is not below a minimum threshold.

1.2 Bragg Crystal Spectrometer (BCS)

Instrument:	Bent Crystal Spectrometers	
Spectral lines:	Fe XXVI (1.76 - 1.81 A)	(Chan 1)
	Fe XXV (1.83 - 1.90 A)	(Chan 2)
	Ca XIX (3.16 - 3.19 A)	(Chan 3)
	S XV (5.01 - 5.11 A)	(Chan 4)
Spectral resolution (l/dl):	3000 - 8000	
Angular resolution:	Full disk	
Best time resolution:	0.125 sec	
Typical time resolution:	3.0 sec in FLARE/HI	

1.2.1 Instrument Modes

The BCS has the capability to bin the different channels in a variety of ways. Each binning group is defined by a separate ModeID. For a given ModeID is it possible to determine how the data original bins were combined before being telemetered to the ground.

1.3 Hard X-Ray Telescope (HXT)

Instrument:	Fourier Synthesis Telescope
Energy bands:	(15 - 100 keV, 4 channels)
	Low 14 - 23 keV
	Medium-1 23 - 33 keV
	Medium-2 33 - 53 keV
	High 53 - 93 keV
Angular resolution:	~5 arcsec
Effective area:	1.5 cm2 avg. x 64 elements
Field of View:	35 x 35 arcmin
Best time resolution:	0.5 sec
Typical time resolution:	0.5 sec in FLARE/HI

1.4 Soft X-Ray Telescope (SXT)

Instrument:	Glancing incidence mirror/CCD sensor
	Co-aligned optical telescope using same CCD

```
Wavelength ranges:   2.5-46 A     no analysis filter (or Noback)
                     2.5-36 A     1265 A Al
                     2.4-32 A     2930 A Al, 2070 A Mg, 562 A Mn, 190 A C
                     2.4-23 A     2.52 micron Mg
                     2.4-13 A     11.6 micron Al
                     2.3-10 A     119 micron Be
                     4600-4800 A  Wide band optical filter
                     4290-4320 A  Narrow band optical filter
Spectral discrimination:   Filters
Angular resolution:        3 arcsec
Field of View:             42 x 42 arcmin
Best time resolution:      0.5 sec
Typical time resolution:   2.0 sec in FLARE, 8.0 sec in QUIET
```

After the failure of an entrance filter in Nov-92, the narrow band, wide band optical filters, and Noback X-ray filter became unusable.

1.4.1 Sequence Tables

SXT uses sequence tables to define the order that the images will be taken. There are thirteen 'slots' which are available to set the parameters. For each slot a separate filter, resolution and observing region can be specified. The observing region selection is from a table of nine entries. Each entry specifies a location and the size of the output image in pixels (this means that the field of view is different depending on the pixel resolution used).

The sequence is started from the beginning whenever the "SXT CNT AUTO" command sequence is issued from the ground or by programmed control, or if the telemetry rate or mode changes. Therefore, the sequence does not automatically begin at the top at the beginning of a new orbit, for example.

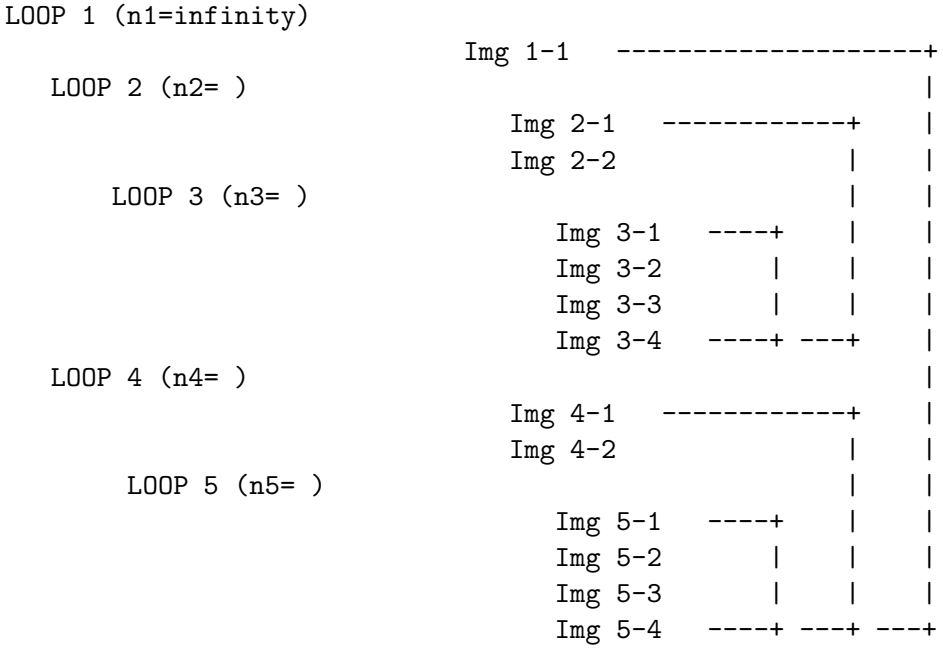

1.4.2 Automatic Exposure Control (AEC)

SXT has automatic exposure control (AEC) available for partial frame images. The algorithm works on a per observing region basis and runs separately for each "slot" shown in the sequence above (image 3-3 exposure control is independent of image 5-3, even if they are for the identical filter and location). An upper and lower intensity, or Data Number (DN), threshold is set and the number of pixels above and below that threshold is set. An allowable number of pixels above and below is also set, and if the image exceeds this set level, then the exposure duration is shortened or lengthed, depending on whether it is over exposed or under exposed. See the "Red Book" article for more details on the exposure control.

1.4.3 Automatic Region Selection (ARS)

The automatic region selection (ARS) allows two different selection methods. ARS-1 takes an exposure of the sun and locates the brightest points and selects the brightest four locations. Normally the sequence table simply uses the single brightest active region. ARS-2 allows the operator to specify a sub-region of the sun, and the tracking algorithm will point to the brightest region within that sub-region. ARS-2 is normally used to force the pointing to stay on a fixed region, and to correct for solar rotation. See the "Red Book" article for more details on the region selection.

1.5 Wide Band Spectrometer (WBS)

```
Instruments:
          Soft X-ray Spectrometer (SXS)
          Hard X-ray Spectrometer (HXS)
          Gamma-ray Spectrometer (GRS)
          Radiation Belt Monitor (RBM)

          SXS: Gas Proportional Counter (3-30 keV (nominal), 128 channels)
          HXS: NaI scintillation counter (20-657 keV, 32 channels)
          GRS: BGO scintillation counter (0.3-100 MeV, 144 channels)
          RBM-SC: RBM NaI Scintillation Detector (5-300 keV)
          RBM-SD: RBM Si Detector (>20 keV)
Angular resolution:     Full disk
Best time resolution:   0.125 sec
```

Most of the sub-instruments have pulse height (PH) data and pulse count (PC) data. PH is essentially a spectrum with counts as a function of energy, and PC is the sum of all counts for a given energy range.

The structure for the WBS data has numerous tags. Some of the data tags and types of data available are listed below.

SXS has two detectors with a 2-channel PC and 128-channel PH for each detector. The energies listed below are nominal values.

```
sxs_pc11 - SXS-1 Detector, chan 1 (3-15 keV)
sxs_pc12 - SXS-1 Detector, chan 2 (15-40 keV)
sxs_pc21 - SXS-2 Detector, chan 1 (3-15 keV)
sxs_pc22 - SXS-2 Detector, chan 2 (15-40 keV)

sxs_ph1  - SXS-1 Detector, 128-channel PH (3-30 keV)
sxs_ph2  - SXS-2 Detector, 128-channel PH (3-30 keV*)
```

HXS has a 2-channel PC and a 32-channel PH.

```
hxs_pc1  - HXS Detector, chan 1
               (20-60 keV for 1-Oct-91 to 9-Jun-92)
               (25-75 keV for 9-Jun-92 to present)
hxs_pc2  - HXS Detector, chan 2
               (65 - 657 keV for 1-Oct-91 to 9-Jun-92)
               (75 - 830 keV for 9-Jun-92 to present)

hxs_ph   - HXS Detector, 32-channel PH
               (20 - 657 keV for 1-Oct-91 to 9-Jun-92)
               (25 - 830 keV for 9-Jun-92 to present)
```

GRS has two detectors with a 6-channel PC and a 128-chan PH (16-channel for the high words) for each detector.

```
grs_pc11  -  GRS-1 Detector, chan 1 (0.27 - 1.04 MeV)
```

```
grs_pc12  -  GRS-1 Detector, chan 2 (1.04 - 5.47 MeV)
grs_pc13  -  GRS-1 Detector, chan 3 (5.47 - 9.3   MeV)
grs_pc14  -  GRS-1 Detector, chan 4 (9.3  - 13.1  MeV)
grs_pc15  -  GRS-1 Detector, chan 5 (8 - 30 MeV)
grs_pc16  -  GRS-1 Detector, chan 6 (30 - 100 MeV)

grs_phl1  -  GRS-1 Detector, 128-chan (0.3 - 13.6 MeV)
grs_phh1  -  GRS-1 Detector, 16-chan (8 - 100 MeV)

grs_pc21  -  GRS-2 Detector, chan 1 (0.3 - 1.24 MeV)
grs_pc22  -  GRS-2 Detector, chan 2 (1.24 - 5.66 MeV)
grs_pc23  -  GRS-2 Detector, chan 3 (5.66 - 9.37   MeV)
grs_pc24  -  GRS-2 Detector, chan 4 (9.37  - 13.6  MeV)
grs_pc25  -  GRS-2 Detector, chan 5 (8 - 30 MeV)
grs_pc26  -  GRS-2 Detector, chan 6 (30 - 100 MeV)

grs_phl2  -  GRS-2 Detector, 128-chan (0.3 - 13.6 MeV)
grs_phh2  -  GRS-2 Detector, 16-chan (8 - 100 MeV)
```

RBM has two detectors. RBM-SC has 2-channel PC and 32-channel PH, and RBM-SD has 1-channel PC.

```
rbm_sc_pc1 - NaI scintillation detector (5-60 keV)
rbm_sc_pc2 - NaI scintillation detector (60-300 keV)
rbm_sd_pc  - Si detector (>20 keV)
rbm_sc_ph  - RBM-SC Detector, 32-chan (5-300 keV)
```

1.6 Spacecraft Attitude Control System (ACS)

The attitude control system uses momentum wheels, magnetic torquers, and control-moment gyros as the actuators. As the attitude sensors, two sun sensors and a star tracker, as well as geomagnetic sensors, are available for determining the spacecraft pointing relative to the direction of the sun and to the ecliptic plane, respectfully. An inertial reference unit comprising four gyros detects changes of attitude with time.

2 Bragg Crystal Spectrometer (BCS)

The Bragg Crystal Spectrometer (BCS) is designed to study plasma heating and dynamics during the impulsive phase of solar flares. It consists of two bent crystal spectrometers, BCS-A and BCS-B, that observe the H-like line complex of Fe XXVI, and He-like complexes of Fe XXV, Ca XIX and S XV. Each spectrometer consists of a double detector placed behind a pair of germanium crystals that diffract the incoming X-rays into the detectors. The two structures are mounted at the front of the Yohkoh spacecraft, on either side of the central panel, with a thermal filter mounted in front of each spectrometer. The crystal dispersion axes are oriented north-south.

There is much more about the performance of the BCS instrument than is reported here. If additional information on the design and performance of the BCS is needed, the user is encouraged to consult the documents listed in Section **??**.

2.1 Instrument Characteristics

2.1.1 Wavelength Range

The designed and laboratory measured wavelength ranges are given in the table below:

Chan	Designed Wavelength	Bin Range	Lab. Measured Wavelength
1	1.7636 -- 1.8044	212 -- 28	1.7597 -- 1.8121
2	1.8298 -- 1.8942	224 -- 36	1.8284 -- 1.8957
3	3.1631 -- 3.1912	27 -- 229	3.1633 -- 3.1933
4	5.0160 -- 5.1143	40 -- 234	5.0163 -- 5.1143

It should be stressed that these wavelengths are only valid at the designed, nominal BCS boresight. Because of the nature of the way a bent crystal spectrometer works, if a source is observed at other than the boresight then the wavelength range observed by the detector is shifted. In order to allow the SXT to observe more of the northern polar corona, the Yohkoh spacecraft is normally pointed several arcmins north of its designed pointing; because the dispersion axes of the crystals are oriented in the north-south direction, with this offset pointing channels 1 and 2 are normally seeing wavelengths that are slightly shorter than designed, and channels 3 and 4 slightly longer than designed. Consequently, during times of the year when the north pole of the Sun is tilted towards the Earth (i.e. Oct-Jan), if the active region is in the southern solar hemisphere, then this offset pointing severely compromises the ability of the BCS to observe the blue-wing in Ca XIX (channel 3).

The bin shifts caused by an offset in the pointing were measured in the laboratory to be (6.634±0.039) 10^{-2} bins/arcsec, (4.730±0.025) 10^{-2} bins/arcsec, (8.218±0.062) 10^{-2} bins/arcsec and (4.305±0.028) 10^{-2} bins/arcsec for channels 1 to 4 respectively (note: these are per single bin — channels 3 and 4 are often double binned). These values are being confirmed by in-orbit measurements which compare the bin of the resonance line with the source position observed by SXT. The above values correspond to 15.074, 21.142, 12.168 and 23.229 arcsec/bin.

2.1.2 Data Compression

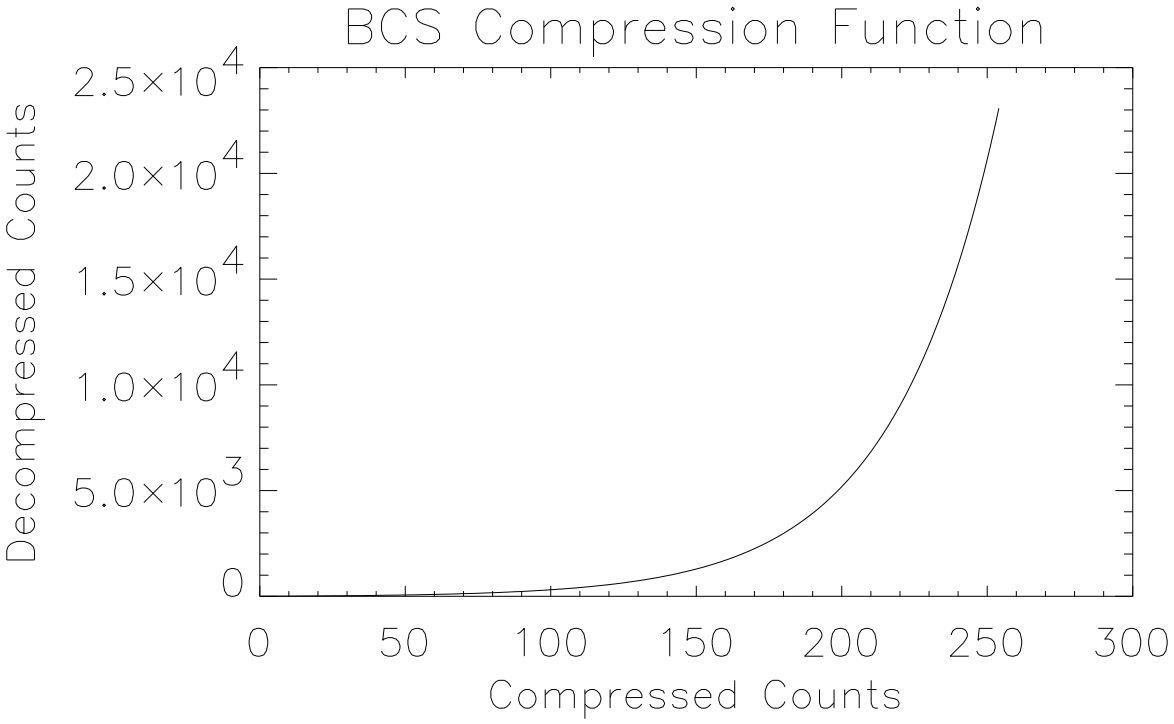

Figure 2.1: The BCS data compression algorithm

All the BCS spectral data are output to telemetry as compressed counts. The compression is done by a hardware lookup table held in ROM (read-only memory) using a compression scheme that minimizes the errors. It is a complex function and is shown in Fig **??**.

2.2 Instrument Calibration

The BCS instrument was calibrated at the Rutherford Appleton Laboratory (RAL). This work is described in Lang *et al.*, 1993.

2.2.1 Sensitivity Functions

The response of a spectrometer channel depends on the transmission of the detector window (as a function of its length), the detector linearity, the crystal curvature and the transmission of the thermal filter. All three of these factors were independently measured during construction of the BCS and an all-up check was then performed at RAL. The response files for each of the channels are in the directory defined by "$DIR_BCS_CAL" under the names BCSA1.nnn, BCSA2.nnn, BCSB3.nnn and BCSB4.nnn, where nnn is the file version number. The sensitivity functions contained in these files are listed in tables in an appendix of Lang *et al.*, 1993.

These functions represent the departure from the nominal efficiency, or effective area of the spectrometers. The measured effective areas, with uncertainties, for the flight wavelength ranges are 0.104±0.009 cm^2, 0.114±0.012 cm^2, 0.303±0.032 cm^2 and 0.071±0.010 cm^2 for channels 1 to 4 respectively when the relative response within a channel is taken to be uniform.

2.2.2 Wavelength Resolution

The wavelength resolution for a particular BCS channel depends on the rocking curve of the crystal for that channel, on the position resolution of the detector, and on the angle that the photons enter the detector in that channel. The latter point is more relevant to the higher energy photons of channels 1 and 2 — these photons penetrate further into the detector volume and if their path is not perpendicular (to the window) they will produce an electron cloud that spans a longer length of the wedge-and-wedge cathode, and hence a broader positional distribution.

2.3 Detector Performance

2.3.1 Detector Gain and Energy Resolution

The gain and energy resolution of the detectors are dependent on the gas mixture and the high-voltage (HV) setting. The detector performance is regularly checked using a Fe^{55} radioactive source. There are 8 setting of the high voltage at 30 volt intervals that can be used to compensate for changes in the detector gain due to contamination (gain decreases) or leakage (gain increases) — each step represents a change of a factor of ∼1.28 in gain. The trims on both HV units were set to the nominal value of 4 (1476 V) at launch. Although both detectors are showing a small, steady decrease in gain (1.95% p.a. in BCS-A and 0.92% p.a. in BCS-B), it has not yet been necessary (Jan/94) to change the HV trim setting. The history of the HV trim settings are contained in file "$DIR_BCS_LOGS/hv_log.dat" .

During the radioactive source calibration, in order to make it possible to detect the 5.9 KeV photons emitted by the Fe^{55} source, the gain of the detector for BCS-B is changed by setting an HV trim level of 2 (1418 V).

The results of the PHA (pulse-height analyzed) pre- and post-launch detector calibrations performed with a radioactive source are contained in the file "$DIR_BCS_LOGS/gain_log.dat." A history of the the gain and energy resolution of the two BCS detectors can be obtained by typing the IDL command:

IDL> **.run gain_plot4**

The variation of the gain with temperature (determined from measurements made during the pre-launch Thermal Test) can be obtained by typing the IDL command:

IDL> **.run gain_temp_plot**

2.3.2 Position Resolution

The position resolution of channels 1 and 2 are approximately 350 μm, and channels 3 and 4 somewhat larger.

The wedge-and-wedge pattern of the detector can be stimulated through a set of three pads located on the rear of the quartz plate. When a signal is applied to a pad, it induces a charge on the pattern in the same way that an incoming photon would, but at a known location. During a stim test, each pad is stimulated in turn. The position resolution and linearity of the detectors are regularly measured using these electronic stims.

2.3.3 Digitization Spikes

The position of a photon in the detector is calculated from the signals measured on the two wedges (W_a and W_b) of the wedge-and-wedge cathode. The position is given by the formula:

$$x = \frac{W_a}{W_a+W_b}$$

In the BCS this calculation is done using a look-up table held in ROM. Because of the quantized nature of this digital technique, solutions sometimes fall either side of the value that would have been determined with an analogue technique and spikes and dips are seen in what should be a flat field. The position of these can be calculated, and corrected — there is some dependence on the energy of the detected photon. No photons are lost, they are merely displaced into adjacent bins so integrations under curves are not affected, but when fitting spectra it is best to avoid those bins.

2.4 Detector Background

2.4.1 Energy Discrimination

To allow the rejection of photons whose energies lie outside the desired range, a pair of adjustable energy discriminators (single channel analyzers, or SCA's) are provided for each channel of the BCS.

The history of the SCA settings are contained in file "$DIR_BCS_LOGS/sca_log.dat".

2.4.2 Particle Background

The BCS detectors are effected by a background caused by particles trapped in the Earth's magnetic field. Many of these are rejected by the setting of the lower level SCA, but occasionally some are seen in channels 1 and 2 – they appear as a flare-like spike, but are not seen at the corresponding time in channels 3 and 4.

Over the South Atlantic Anomaly, the background caused by trapped particles is particularly intense and the High Voltage supplies to the BCS detectors are switched off (using time-tagged commands).

2.4.3 Germanium Fluorescence

When germanium is illuminated by photons whose energy exceeds 11.2 keV, the crystal fluoresces, emitting a photon whose energy is 9.9 keV. Since the energy resolution of the BCS detectors is around 20%, the tail of the distribution of these fluorescent photons falls within the energy range that the BCS is sensitive to and indeed part of the tail lies under the distribution of the photons detected by channels 1 and 2. In order to try to reject the fluorescence, the upper level discriminator is set midway between the two energy distributions. germanium fluorescence is less of a problem in channels 3 and 4 since there is a greater difference in the energy between the channel photons and the fluorescent photons.

2.4.4 Effect of Gain Depression

When the observed count rate increases the gain of the detector becomes depressed and the position that the photons from a given channel are recorded at (in SCA space) slips to lower values. As a consequence, the perceived energy distribution of the photons can move relative to the energy window defined by the lower and upper level discriminators and some photons

may be rejected as being out of limits. This effect has made it difficult to reject the photons caused by Ge fluorescence when the count rates are high.

2.5 Dynamic Range and Count Rate Effects

The dynamic range of a proportional counter of the type used on the BCS is limited and it is not possible to observe both very weak and very intense flares. The BCS on Yohkoh was designed to have high sensitivity so that it can observe as early as possible at the onset of a flare and the dynamic range is therefore biased towards the smaller flares. As a consequence the BCS saturates during larger flares, i.e at high count rates. During saturation all positional information is lost but the total event counter may still be valid.

2.5.1 Deadtime Correction

All analogue signals produced by the detectors take a time to process that is significant when count rates are high. Although the anode signals only take 1 μs to process, the processing of the wedge signals takes 3.5 μs and additional time needs to be allowed for the signal levels to settle back to zero so that in total 35 μs must elapse between successive photons. Consequently, during this "deadtime" the processing of any new position signals is inhibited. At low count rates this effect is small, but it becomes more important as the count rate increases. If the photon arrival times were evenly spaced, then the pair of channels in one detector could see a maximum of $\sim 28 \times 10^4$ counts/sec. However, in practice the random nature of the events, and the onset of saturation, results in a maximum of less than half this.

In the BCS there are three sets of counters for each channel: the total event counter, the limited (or in-window) event counter and the encoded event counter. The gate for the limited event counter only accepts events that fall within the allowed energy window, and in addition inhibits any event that arrives less than 35 μs after the previous one. From a knowledge of the event counters, it is possible to calculate the effects of the deadtime and hence reconstruct what the count rate should be. This is done within the MK_BSC and MKBSD routines.

It should be noted that while the event counters used for deadtime corrections are in the DP-synchronous (DP_SYNC) part the telemetry, the spectral data are in the PH stream and after passing through the queue memory are asynchronous. As a consequence, if there are holes in the data coverage, it is possible for the DP_SYNC data to be absent at the time of the spectral observations. At such times it is not possible to make a deadtime correction.

2.5.2 Saturation

The problem of saturation is exacerbated by the double detectors used on the BCS. During construction, constraints on mass and volume required that the two channels on a spectrometer shared the same detector gas volume. Although the anode signals from the detectors (which allow energy discrimination) are processed separately for each channel, the positional information is provided by a wedge-and-wedge pattern that is shared by the channels. Thus, the processing deadtime for position encoding for a detector is affected by the sum of the total count rates for both channels of that detector.

That the onset of saturation is determined by the counts in two channels can produce "interesting" effects. For instance, if the flare is hot, the detector of spectrometer BCS-B will saturate at a higher count rate in Ca XIX (channel 3) than if it is cool. Normally the count rate in S XV (channel 4) will dominate in BCS-B, but for a hot flare the saturation will depend more on the Ca XIX than on the S XV count rate. In spectrometer BCS-A, Fe XXVI (channel

1) has only been observed in a few flares because often the count rate in Fe XXV (channel 2) is already very high by the time that Fe XXVI is likely to be observed.

It should be noted that adjusting the SCA values does not affect the onset of saturation. The same number of photons are still entering the detector and each is seen by the positional encoding circuitry no matter how many are gated as having valid energies.

2.5.3 Gain Depression

As mentioned under the "Detector Background" section, when the count rate is high, the gain of the detector becomes depressed and the perceived energy distribution slides down in the SCA space, and possibly partly or totally out of the energy window set by the SCAs. As a consequence, the number of photons accepted as having valid energy is reduced and since this signal is used to determine whether the decoded position should be used, the number of encoded photons is reduced.

2.5.4 Rate-dependent Distortion

When a large number of counts are put into a small length of the detector volume, a space charge effect develops which attracts the electron cloud towards that region of the detector. This results in lines that are taller and narrower than they should be and locally distorts the linearity of the detector. This effect is not confined to spectral lines and can occur in any region of the detector where the photon flux is large; the total number of counts is conserved, but there is a loss of positional information. It is not clear that this effect can be deconvolved, and the matter is still being studied. More information is given in Trow, Bento and Smith (1993).

2.6 Data Features

2.6.1 Queued Data

The BCS spectral data are stored in a queue memory prior to insertion in the telemetry frame. These data are therefore asynchronous to the data in the DP synchronous area of telemetry and occasionally the DP_SYNC data are not present at the same times as the spectral data. During these periods, deadtime correction to the spectral data are not possible. Key items relating to the mode being executed by the BCS are included in header information included in the queued data and it is always possible to know what mode the BCS is in.

At times a mode called "Fast Queue" is used. In this the data accumulators are sampled at intervals without clearing and then the data are stored in two different queue — normal and fast. The final integration before clearing of the accumulator is stored in the normal queue and all others are stored in the fast queue. In this mode, if the flare-flag is raised the fast queue is dumped to telemetry, but normally only data from the normal queue goes into telemetry. The mode is used at times when the spacecraft is in a mode whose bit-rate does not allow as short an accumulation time as is desired. The fast queue allows high cadence data to be stored and only output if a flare switches the spacecraft to a higher bit-rate.

Fast Queue data can be recognized by a sawtooth-type ramping in the light curve. These type of data are normalized by the IDL function BCS_NORM.

2.6.2 Timing of Spectra

The time contained in a mode record for a BCS spectrum represents the start of the integration time of that spectrum. Thus a correction (equal to half the integration period) needs to be

added to the points in a light curves for all plots that are NOT in histogram mode (psym=10). The routine BCS_TVEC does this.

2.6.3 Last Spectral Bin

The last bin in each channel is used to accumulate positionally encoded counts when the sum of the signals on the two wedge, or the signal on any individual wedge is very small or very large. Although useful as a diagnostic, these bins should ignored for analysis purposes.

2.6.4 Medium-rate Spectral Data in Autumn 1991

Just after the launch of Yohkoh, it was found that there was an error in the way the DP inserted BCS PH-data into the telemetry frame during medium bit-rate. This can be seen a "hole" that steadily marches through the data in successive spectral integrations; when viewing the light curve, a periodic, but structureless reduction in the count rate is seen in medium bit rate. When the hole is not in an interesting part of the spectrum, the data can be used, otherwise it should be rejected. The problem was corrected by a patch to the DP in late November 1991.

2.6.5 Single Event Upsets

At intervals, and particularly when the spacecraft has its apogee over the South Atlantic, the memory of the BCS microprocessor can be corrupted by a Single Event Upset (SEU). Often this affects a part of the memory that does not disturb the running of the BCS, but whenever an SEU is detected (most are flagged as a result of a checksum calculation), the BCS microprocessor is rebooted. Occasionally, several hours, or days of data have been lost before this is done.

2.7 Contact Persons

If you have any question about BCS software and/or instrument, or if you need any advice in BCS data analyses, contact:

`yla@solar.physics.montana.edu`

2.8 References

- "BCS Experiment Users Guide", ed. K. J. H. Phillips.
- J. L. Culhane et al., "The Bragg Crystal Spectrometer for Solar-A," 1991, Sol. Phys. 136, 89.
- J. Lang *et al.*, "The Performance of the Bragg Crystal Spectrometer," 1992, P.A.S.J. 44, 5, L55.
- J. Lang, *et al.*, "The Laboratory Calibration of the Yohkoh Bragg Crystal Spectrometer," 1993, RAL Publication RAL-93-035.
- M. W. Trow, R. D. Bentley and J. L. Culhane, "A Positional Sensitive Proportional Counter for the Bragg Crystal Spectrometer on Solar-A," 1989, SPIE 1159 EUV, X-ray and Gamma-Ray Instruments for Astronomy and Atomic Physics, 252.
- M. W. Trow, A. C. Bento and A. Smith, "Rate Dependent Image Distortions in Proportional Counters," 1993, Nucl. Inst. & Meth. A, in press.

3 Hard X-Ray Telescope (HXT)

3.1 Overview

HXT is a Fourier synthesis type imager consisting of 64 bi-grid modulation subcollimators (SC's). Each SC has a different pitch and/or a position angle of collimator grids, together with a NaI (Tl) scintillation crystal and a detector photomultiplier located behind the SC. The number of hard X-ray photons passing through a single SC is periodically modulated with respect to the incident angle, which gives a modulation pattern of the corresponding SC, and count rate data obtained by each detector which can be regarded as a spatial Fourier component (+ DC level) of a hard X-ray image.

When a flare-mode is triggered, a set of 64 hard X-ray count rate data is accumulated every 0.5 s (= the highest temporal resolution) in four energy bands between 14 and 93 keV (L, M1, M2, and H bands, respectively) and is transferred from HXT to the Data Processor (DP). The data are then telemetered down to the ground and hard X-ray images can be synthesized using image restoration procedures such as the Maximum Entropy Method (MEM).

The field-of-view (FOV) of HXT is about $35' \times 35'$, i.e. covering the whole Sun. This means that HXT can detect hard X-rays of flares regardless of their position on the Sun without re-pointing the spacecraft. The basic image synthesis FOV of HXT is $2'06'' \times 2'06''$ with the angular resolution as high as approximately $5''$. A detailed description on the overview of the instrument is given by Kosugi *et al.* (1991). See Kosugi *et al.* (1992) for the in-orbit performance of HXT as well as some initial results.

3.2 General information

3.2.1 Observations with HXT

Unlike SXT, HXT is operated in a single observation mode (except for calibration). When the Sun is quiet (i.e. in the quiet-high or quiet-medium mode), only hard X-ray count rate data in the lowest energy band (L band; see section 2-2) are telemetered once in every major frame (e.g. 2-s data accumulation in high-bit rate). When the flare-high mode is (automatically) triggered by the occurrence of a flare, then count rate data in the four energy bands, with a 0.5-s data accumulation, are telemetered to the ground. In this case, four sets of data ((64 SC's $\times$ 4 energy bands)$\times$ 4) have their telemetry allocation in one major frame.

When the spacecraft is in South Atlantic Anomaly (SAA) or in spacecraft night, high voltage supplies for the detector photomultipliers are reduced and no solar observations are made with HXT.

3.2.2 Detector gain calibration

Since HXT images are synthesized from sets of data from the 64 SC detectors, it is essential that the gain of each detector be set equal to each other with high precision (within 1 %). The gain calibration of HXT is conducted typically once in a month and the gain has been set constant since the beginning of HXT observations in October 1991, which enables us to obtain reliable hard X-ray images in the four energy bands.

In the calibration mode of HXT (HXT-CAL or Pulse Height (PH) mode), X-ray count data in 64 energy channels between 14 and 93 keV for each detector, instead of four energy bands in the case of observation mode (Pulse Count (PC) mode), are obtained. The gain of each

detector is monitored by accumulating X-rays from an Am-241 calibration source (whose line profile peaks at 59.5 keV) attached on an aluminum case for the NaI (Tl) crystal.

The energy-channel relationship to which detector gains are adjusted is given as follows:

$$E = 1.252 \times (Ch + 10.1)(\text{keV}), where \;\; 0 \leq Ch < 64$$

In normal observation mode, the four energy bands, L, M1, M2, and H, have the following energy range:

Energy Band	*PH Ch*	*Energy Range (keV)*
L	1 - 7	13.9 - 22.7
M1	8 - 15	22.7 - 32.7
M2	16 - 31	32.7 - 52.7
H	32 - 63	52.7 - 92.8

NOTE: Ch=0 is not included in the L band.

3.2.3 Background counts

Even when the Sun is quiet, there are some counts in the four energy bands due to X-rays from the calibration sources, as well as e.g., cosmic X-ray radiation. For a better HXT data analysis, we recommend you carefully subtract non-flare background from flare data you are going to analyze. The typical background (BGD) count rates in the four energy bands are:

Energy band	*BGD count rate (cts/s/SC)*
L	~ 1
M1	~ 2
M2	~ 1
H	~ 8

One must be careful since the above BGD count rates have an orbital dependence; for example, the NaI scintillators are activated during SAA passages and there are some excess counts in the four bands even after exit from SAA. The most suitable way for background subtraction that we recommend at present is to use data just before or after the flare as BGD.

Background subtraction plays an important role in image synthesis as well as spectral analysis with HXT. This is especially true if you are going to analyze not-so-intense flares. Even for intense flares, image synthesis with inappropriate background subtraction will provide you with images with spurious sources scattered around in the image synthesis FOV.

3.3 Some detailed information

3.3.1 Modulation patterns

Among the 64 grid pairs of HXT, 48 are called Fourier elements whose slit and wire widths are the same to each other while 16 are fanbeam elements whose wire widths are three times larger than their slit widths. See Kosugi *et al.* (1991) for more information on the arrangement of the 64 SC's. Modulation pattern parameters of each SC's, which are necessary for synthesizing images, are listed in a file whose name is obtained by the following command:

IDL> **file = concat_dir('$DIR_HXT_CAL', 'para3.dat')**

In the image synthesis procedure modulation patterns of Fourier SC's are approximated by sinusoidal patterns while those of fanbeam SC's by triangular ones.

3.3.2 Spectral Energy Response

The geometrical area of HXT, which is determined by the (average) transmission of the SC's, is 57.4 cm^2. When considering the spectral energy response of the HXT, the following components need be taken into account:

- thermal shield which wraps around the HXT collimator body
- grid wires made of tungsten (for top and bottom grid assemblies)
- face plates made of Carbon Fiber Reinforced Plastic (CFRP) for top and bottom grid assemblies)
- aluminum cases for NaI (Tl) scintillation crystals
- NaI (Tl) scintillation crystals

The spectral energy response for HXT, with the effect of K-escape of tungsten at 69.6 keV and measured energy resolution of NaI (Tl) + photomultiplier tubes taken into account, are summarized in a file whose name is obtained as follows:

IDL> **file = concat_dir('$DIR_HXT_CAL', 'possi4.dat')**

A concise summary of the energy spectral response, together with some useful figures, is provided in "The Yohkoh HXT Databook (I)."

3.3.3 Pre-storage of HXT data in DP

See the Instrument Guide Appendix section **??** for a description of the time delay in the HXT data.

3.3.4 Data compression

Each hard X-ray count rate measurement transferred from HXT to the DP consists of 12-bits. The data are then compressed into 8-bits in the DP according to the following rule:

```
m = n                    (n =    0-  15),
m = int(4 x sqrt(n))     (n =   16-4080),
m = 255                  (n = 4081-4095),
```

where *int(n)* represents the truncated integer value of n. Count rate data for HXT telemetered down to the ground (as well as the variable *data* which is obtained by reading the HXT reformatted database with YODAT) are the compressed numbers; they need be decompressed before starting any analyses on HXT. Decompressed HXT data are obtained by the following command:

IDL> **decomp_data = hxt_decomp(data)**

3.4 Contact Persons

If you have any question about HXT software and/or instrument, or if you need any advice in HXT data analyses, contact:

yla@solar.physics.montana.edu

3.5 References

- Kosugi, T., Makishima, K., Murakami, T., Sakao, T., Dotani, T., Inda, M., Kai, K., Masuda, S., Nakajima, H., Ogawara, Y., Sawa, M., and Shibasaki, K. 1991 : Solar Phys., 136, 17.
- Kosugi, T., Sakao, T., Masuda, S., Makishima, K., Inda, M., Murakami, T., Ogawara, Y., Yaji, K., and Matsushita, K. 1992 : Publ. Astron. Soc. Japan, 44, L45.
- The Yohkoh HXT Databook (I) National Astronomical Observatory, Feb.1993.

4 Soft X-Ray Telescope (SXT)

The following sections are intended as an extension of the "Red Book" paper which describes the fundamentals of the Soft X-ray Telescope (SXT). We strongly recommend that first time users read "The Soft X-Ray Telescope for the Solar-A Mission" which is in Solar Physics 136, pp 37-67.

Many sections in this chapter refer to the SXT Calibration Notes. A partial set of these notes can be found in the $DIR_SXT_DOC directory. Users should send a mail message to the account specified in the preface of this document if they want copies of the notes.

4.1 Overall Response Function for SXT

The SXT response functions have been characterized for a solar thermal spectrum as observed in each of the SXT analysis filters. The SXT is a broad-band instrument and is sensitive over a range of energies between approximately 0.28 and 4 keV. The analysis filters have been carefully selected so that their intensity ratios are diagnostics of temperature.

4.1.1 CCD Camera Signal

The SXT makes use of a front-illuminated, virtual-phase CCD to detect both X-ray and visible photon fluxes. While it is possible to operate CCDs in a photon counting mode, the SXT CCD is operated in a camera-integrating mode. This means that the shutter is opened for a short interval during which photon events are summed into the CCD's pixels. The amount of charge read out of the CCD by the camera represents the energy in the photon flux which has been integrated in each pixel, not the actual number of photons. If the incident beam is mono-energetic, then the amount of charge is directly proportional to the photon flux. However, since the Sun's X-ray flux is far from mono-energetic, we must model the response of the CCD for a given solar spectrum.

When a photon is absorbed in the CCD it produces electron-hole pairs in the silicon. The number of photons, $N(\gamma)$ that produced the charge or number of electrons, $N(\mathrm{e}^-)$, which is read out of the CCD is given by

$$N(\gamma) = \frac{\lambda}{12398.5\,\mathrm{eV}} \times 3.65\,\mathrm{eV/e^-} \times N(\mathrm{e}^-),$$

where λ is the incident photon wavelength (Å) and 3.65 eV/e^- is the energy required to produce one electron-hole pair in silicon. Note that this relation applies only to X-ray energies. The SXT CCD pixels have a full-well capacity of about 250,000 e^- per pixel.

The CCD camera electronics contain analogue-to-digital converters. In this Guide the digital camera output is referred to as DN or Data Number. These values are read from the camera with 12-bit accuracy, but in the case of X-ray images, are compressed to 8-bit values using a

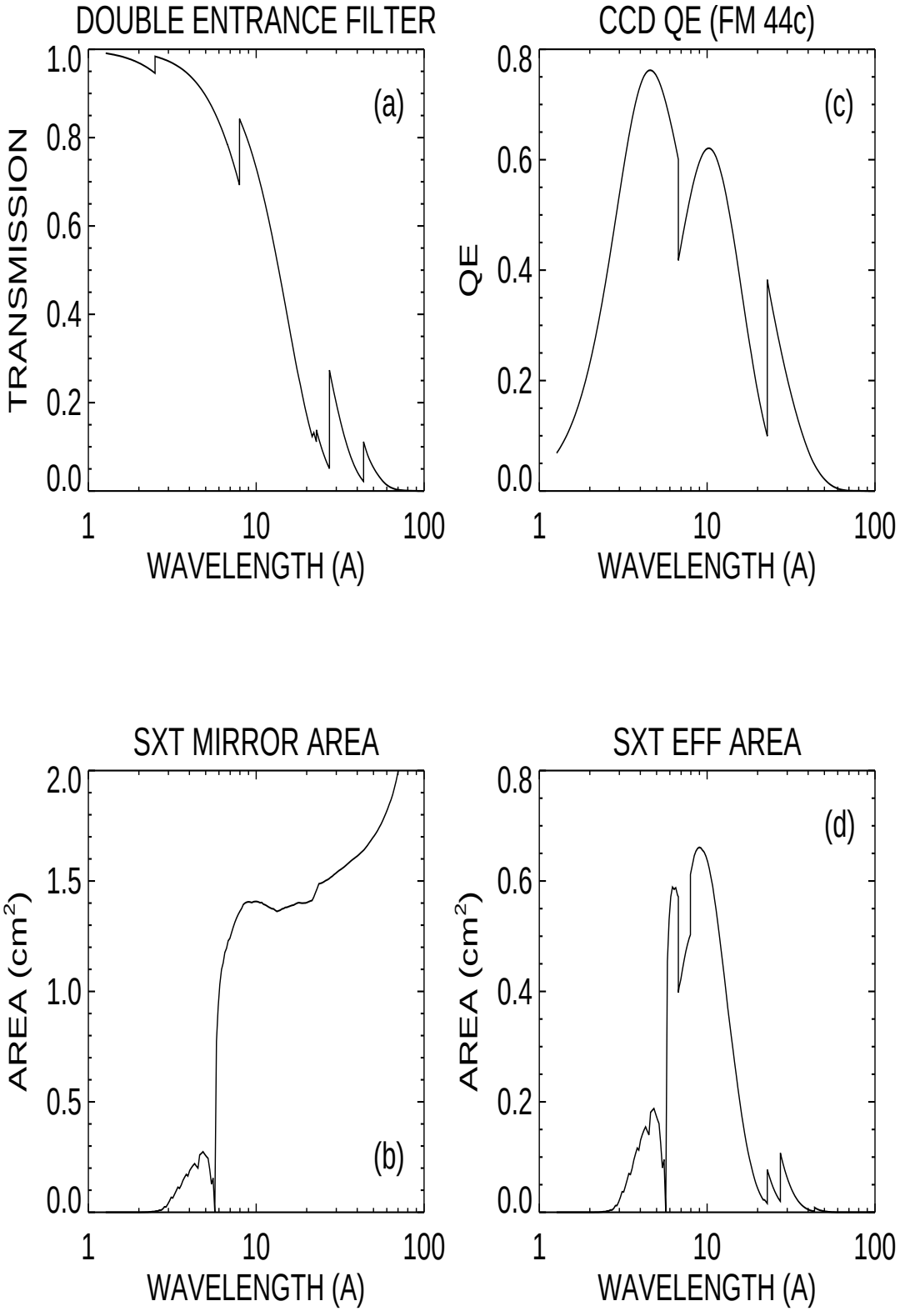

Figure 4.2: Factors that determine the SXT effective area. Panel (a) shows the double entrance filter transmission; panel (b) shows the mirror reflectivity including the obscuration from the support structures; panel (c) shows the CCD quantum efficiency. Panel (d) is the product of panels (a), (b), and (c).

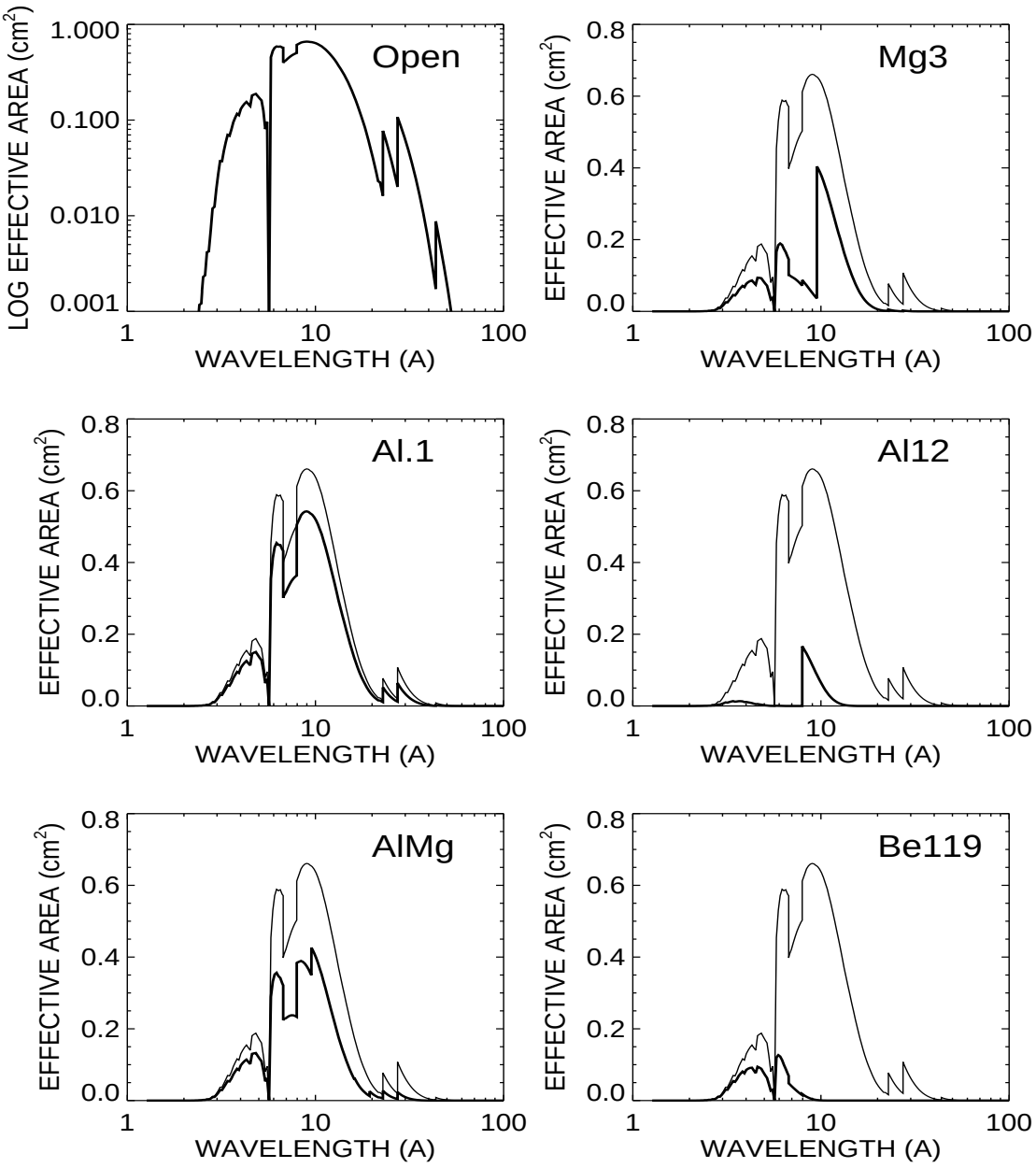

Figure 4.3: The effective area of the SXT: The thick curve shows gives the effective area for the indicated filter. The thin curve is the open filter case (no analysis filter) effective area over-plotted for comparison.

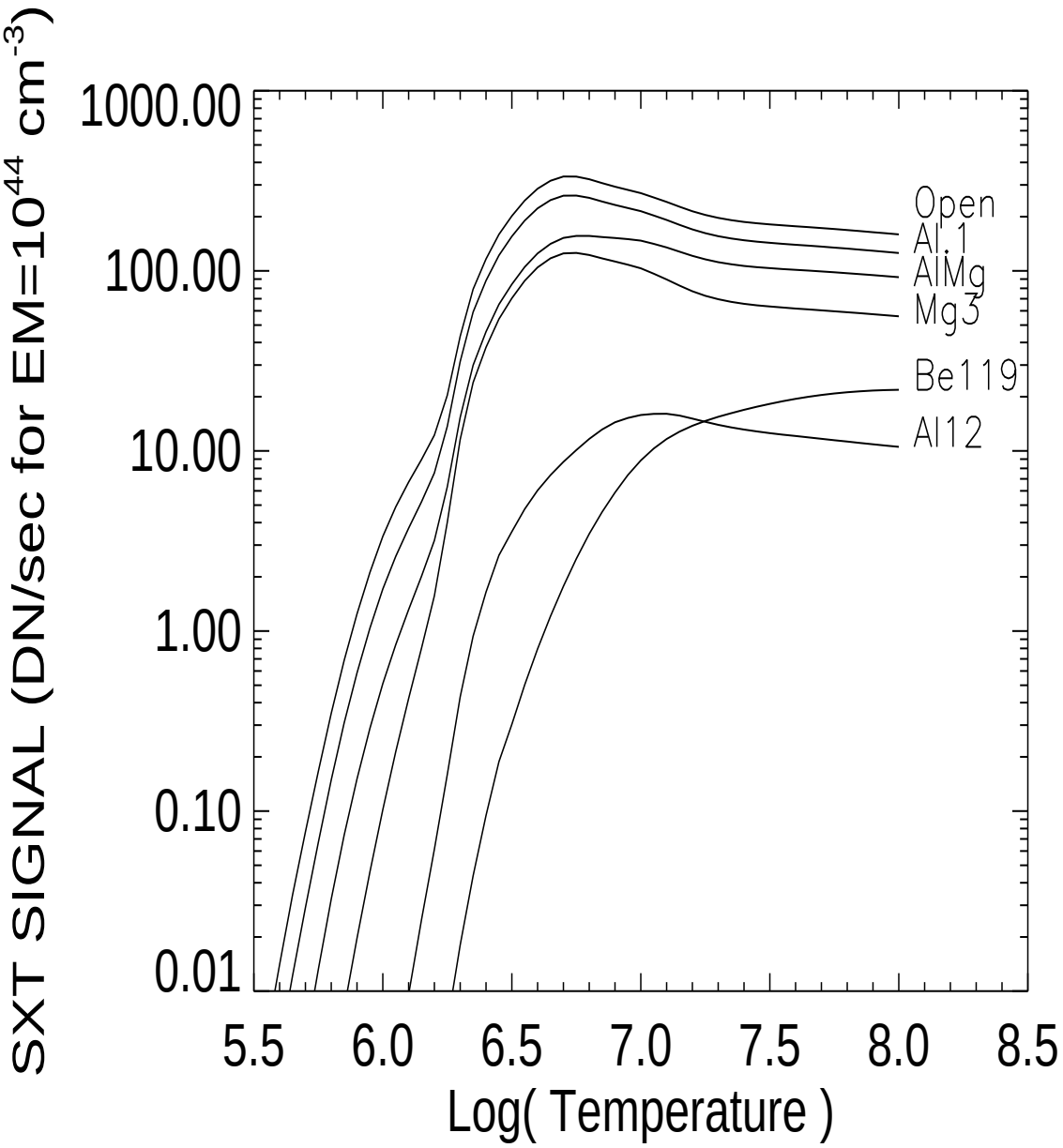

Figure 4.4: The total SXT signal as a function of $\log_{10}(T_e)$ for the open filter and the analysis filters as indicated. NOTE: Be and Al12 are mistakenly reversed in Tsuneta *et al.*, (1991).

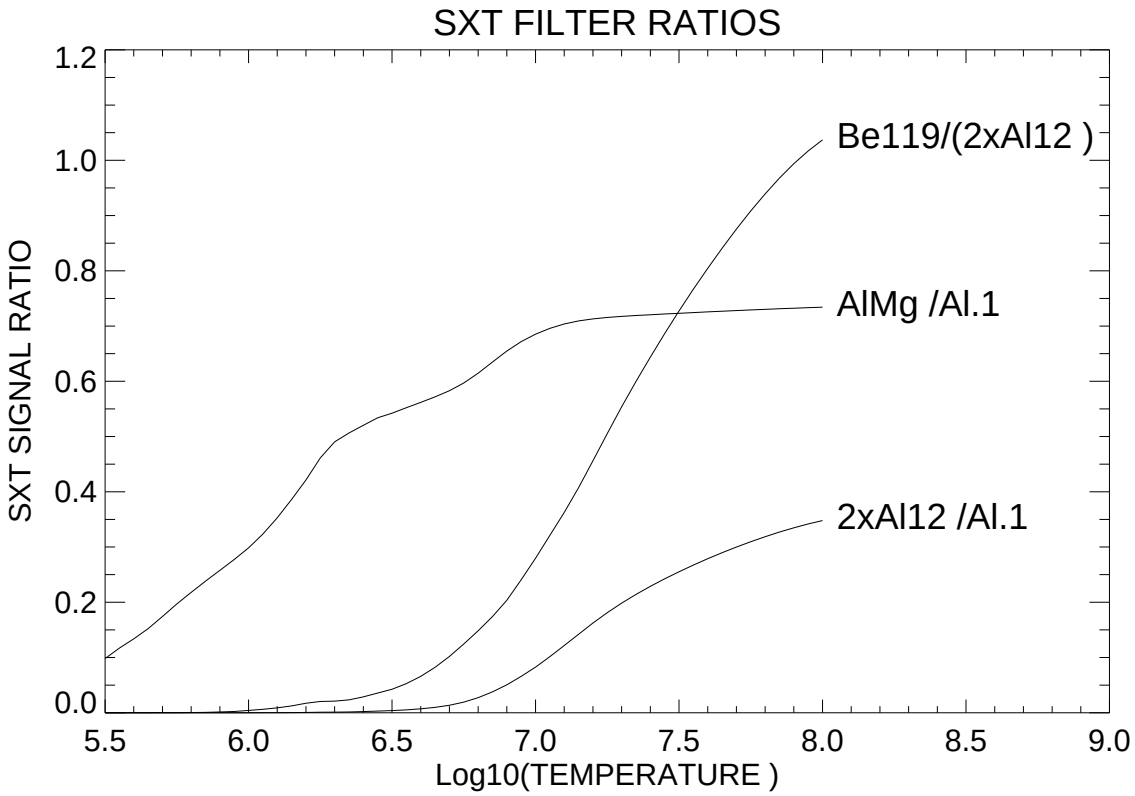

Figure 4.5: Ratios of the SXT response functions. For the curve marked "Be119/(2×Al12)" the effective observing time with the Al12 filter has been doubled with respect to the Be119 filter. For the curve marked "2×Al12/Al.1" the effective observing time with the Al12 filter has again been doubled, this time with respect to the Al.1 filter.

pseudo-square root compression algorithm prior to being telemetered. Thus, when looking at raw SXT images, one should remember that the intensity values are typically compressed. The relation between the DN values and the integrated charge or number of electrons is given by

$$\mathrm{DN} = N(\mathrm{e}^-)/G + 13,$$

where G (e^-/DN) is the so-called gain constant and 13 is a digital offset in the CCD camera for full resolution images (see Section **??** for more information). The value of G was adjusted to be about 100 e^-/DN prior to launch. This value is a compromise to enable adequate performance at both X-ray and visible light energies. The routine SXT_DN2PH will convert SXT DN values into photon counts for a user-supplied wavelength. The digital offset is removed automatically during dark frame subtraction (SXT_LEAKSUB, SXT_DARKSUB), since the dark frame images also have the same digital offset.

4.1.2 SXT Effective Area

The effective area of the SXT to X-rays is described more fully in SXT Calibration Note 31 (J. R. Lemen, 11 Feb 93, Rev A) and also in SXT Calibration Notes 30 and 25.

The on-axis effective area of the SXT depends on four different factors: the double entrance filter transmission, the mirror reflectivity, the analysis filter transmission, and the CCD

quantum efficiency (QE). All these factors are functions of wavelength and off-axis angle (see section **??**). Fig. **??** (a) shows the double entrance filter transmission, Fig. **??** (b) shows the mirror reflectivity (including the effects of obscuration by the support structures), and Fig. **??** (c) shows the CCD QE as a function of wavelength. Fig. **??** (d) shows the product of Figs **??** (a)–(c) and corresponds to the SXT effective area when both filter wheel positions are "open" and sometimes referred to in SXT documentation as "noback" (for no back filter). Fig. **??** contains six panels which show the SXT effective area through the open position and through each of the X-ray analysis filters. Calibration Note 31 gives details about how these curves were derived, but in short, measurements were made a selected wavelengths, to which model calculations were fit and used to predict the responses at any desired wavelength. NOTE: Be and Al12 are mistakenly reversed in Tsuneta *et al.* (1991) for Fig **??**.

4.1.3 Reading the SXT Effective Area File

Although it is not normally necessary to access the effective are data file directly, it is very easy to do so. In IDL you must type:

```
IDL> file = CONCAT_DIR('$DIR_SXT_SENSITIVE','sra930211_01.genx')
IDL> restgen,file=file, str=area
IDL> help,area,/str

** Structure MS_125793397004, 5 tags, length=11600:
   WAVE            FLOAT     Array(290)
   ENTRANCE        FLOAT     Array(290)
   CCD             FLOAT     Array(290)
   MIRROR          FLOAT     Array(290)
   FILTER          FLOAT     Array(6, 290)


IDL> plot_oi,area.wave,area.entrance,xr=[1,100]
IDL> plot_oo,area.wave,area.filter(0,*),xr=[1,100],yr=[.001,1]
```

The last two plot commands will reproduce Fig. **??** (a) and the first panel in Fig. **??**, respectively. In the data structure, *WAVE* is a vector of wavelengths, *ENTRANCE* is the double entrance filter transmission, *CCD* is the CCD QE, *MIRROR* is the mirror effective area (including obscuration), and *FILTER* is the effective area through the various filters. The order of the filter data is according to filter thickness going from 0=open to 5=Be119. Note: this is not the normal SXT filter numbering scheme.

4.1.4 SXT Response to Thermal Plasma

The response of the SXT to a thermal plasma has been computed using the thermal spectrum of Mewe *et al.* (1985, 1986), but with the abundances adjusted to coronal values (Meyer, 1985). The SXT thermal responses are shown in Fig. **??** for the various analysis filters. One can see from the curves that there are essentially two "thick" filters and three "thin" filters plus the open position. The open position has almost never been used during flight. This is because, prior to the entrance filter failure in November 1992, the aspect sensor door was left open almost

continuously in order to take optical exposures. After the entrance filter failure in November 1992, the open position became unusable.

The SXT response functions are available through the IDL routine SXT_FLUX. For example,

```
IDL> te = 5.5+findgen(51)*.05                ; Log10(te) vector between 5.5 and 8.0
IDL> plot_io,te,SXT_FLUX(te,1),yr=[.01,1000]
IDL> for i=2,6 do oplot,te,SXT_FLUX(te,i)
```

should reproduce Fig. **??**. Note that the second argument is the normal SXT filter-B number.

1	Open/Open or Noback case
2	Al 1265 Å
3	Dagwood sandwich
4	Be 119 μm
5	AL 12 μm
6	Mg 3 μm

The units of the plot are DN/sec for an emission measure, EM=10^{44} cm^{-3}. SXT_FLUX has an optional switch: */photons*; if specified, the routine will return the equivalent photons s^{-1} detected by the SXT. This will allow the user to determine the value of DN/photon as a function of filter and electron temperature. For example, try the following IDL commands to plot DN/photon for each filter as a function of electron temperature.

```
IDL> plot,te,SXT_FLUX(te,4)/SXT_FLUX(te,4,/photons) ; plot DN/photons vs te
IDL> for i=1,6 do oplot,te,SXT_FLUX(te,i)/SXT_FLUX(te,i,/photons)
```

The partial entrance filter failure in November 1992 caused a small change to the SXT response function. SXT_FLUX has a *date=* option which will return the new response function if the date is given as *date='13-nov-92 17:01'* or later (the date can be given in any standard Yohkoh format, such as a roadmap or index structure). In this case, the fractional open area of the entrance filter (the size of the hole) is taken to be 0.0833.

For information about how to obtain temperature estimates from the intensity ratios through the various filters, see the User's Guide.

4.1.5 Reading the SXT Response Function File

The routine SXT_FLUX reads the thermal response function data from a file. Although it is not normally necessary, the response function file can be read directly using the following commands:

```
IDL> file=concat_dir('$DIR_SXT_SENSITIVE','sre930211_02.genx')
IDL> restgen, file=file, str=response
IDL> help,response,/str

** Structure MS_125794338005, 5 tags, length=5280:
   TEMP            FLOAT     Array(51)
   ELECTS          FLOAT     Array(12, 51)
```

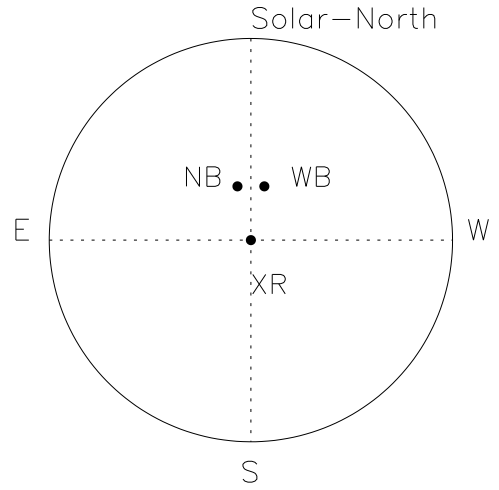

Figure 4.6: Relative alignment of the X-ray and optical images (as of 1992 analysis). According to the final calibration in 2008, the NB and WB boresights are both in the NE of the X-ray boresight.

```
PHOTONS         FLOAT     Array(12, 51)
ELEM            STRING    Array(15)
ABUN            FLOAT     Array(15)
```

Note, that the response file may be updated from time to time. The name contains the date of the last update. In this data structure, the variable *TEMP* is Log10(T_e), *ELECTS* are the number of CCD *electrons* (not DN) per sec for EM= 10^{44} cm^{-3}, and *PHOTONS* is the corresponding number of photons. The first dimension of these two dimensional arrays is arranged so that columns 0 to 5 correspond to the filters in increasing thickness from 0=open to 5=Be119 and assuming the pre-launch entrance filter transmission. NOTE: This is not the normal SXT filter numbering scheme. Columns 6 to 11 correspond to the same filters but with no entrance filter. By combining the corresponding columns in the appropriate ratio, it is possible to quickly compute the SXT response for any size hole in the entrance filter.

4.1.6 Relative Alignment of X-Ray and Optical Images

The relative alignment of the X-ray and optical images is discussed in SXT Calibration Note 36 (R. Fuller, Jan-94). The actual values were initially determined by T. Metcalf in 1992. The final calibration was done by L. Acton in 2008, using all available optical images. The final offset values were determined as:

	x (East/West)	y (South/North)	
NaBan boresight – X-ray boresight	−0.90 (±0.23)	+1.36 (±0.27)	final values (2008)
	−0.36 (±0.18)	+1.47 (±0.28)	old values (1992)
WdBan boresight – X-ray boresight	−0.25 (±0.23)	+1.08 (±0.25)	final values (2008)
	+0.24 (±0.21)	+1.26 (±0.29)	old values (1992)

where values are given in terms of SXT full-resolution (2.453 arcsec) pixels, the negative values indicate East and South, respectively. Fig. **??** shows the relative alignment of the X-ray, narrow band and wide band boresights (as of 1992 analysis). The most current values can be obtained with the routine GT_SXT_AXIS using the command:

```
IDL> print, gt_sxt_axis(1, /rel)        ; NaBan - X-ray
IDL> print, gt_sxt_axis(2, /rel)        ; WdBan - X-ray
```

4.2 The CCD Camera

4.2.1 Saturation Effects

A CCD pixel can contain about 3×10^5 electrons before charge begins to spill into adjoining pixels. This effect is called "pixel saturation". The charge is not lost but appears in pixels surrounding (preferentially above) the saturated pixel. Exact saturation level varies from pixel to pixel but, in general, a signal level of DN=235 (compressed) in a full resolution image is considered to be saturated, i.e., the response of the CCD becomes non-linear. For half and quarter resolution, saturation occurs at DN=255 (compressed). These are the default levels used in SXT_SATPIX which is called by SXT_PREP. It is probable that DN=235 (compressed) is about 5% conservative as histograms of optical images indicate saturation setting in at DN=240 (compressed).

The 12 bit analog-to-digital-converter (ADC) of the CCD camera saturates at about 4.1×10^5 electrons (4095 compressed to DN=255). Charge above this level is lost. Thus, the signal in saturated half or quarter resolution features is a lower limit.

The integrated X-ray intensity in a saturated full resolution image is not lost—only the spatial information is lost. The sum of all of the saturated pixels plus one pixel above (north) and one below (south) yields the integrated intensity of the area thus sampled. Only in very extreme cases does charge spill east or west into adjacent columns. NOTE that the signal in the pixel immediately above and below saturated pixels is questionable as it will usually contain spilled charge. We believe that the difference in saturation level between SXT X-ray and optical images is caused by the charge-spill effect which is not important for optical images — which have much lower contrast.

The routine SXT_SATPIX can be used to flag the location of saturated pixels.

4.2.2 Effect of CCD Contamination

Over time the SXT CCD collects some unknown contaminant. This is still happening, apparently at about the same rate, after more than 2 years in orbit! The problem is first apparent in optical images as noise in the form of short horizontal "dashes" randomly sprinkled over the image. Somewhat later, dark absorption "freckles" appear in the thin filter images at the same location as the "dashes".

The contamination is removed by heating the CCD to +20 C about every 3 months. Sometimes we have waited too long and these contamination artifacts are evident in the images. Although the effect of this contamination on observability of solar features is minimal, we have not yet quantitatively evaluated effects on things like measurement of temperature, emission measure, errors in intensity measurements, etc.

The periods of CCD bakeout are recorded in the appendix of the Reference Guide and can be obtained with the program PR_DATES_WARM. A sample call is:

IDL> **pr_dates_warm**

4.2.3 SXT Images Taken with the CCD Warm

The CCD dark current increases about a factor of 2 for each 8 degree C increase in CCD temperature. The dark current at our normal operating temperature of −20 C is about 1 DN/sec for each full resolution pixel. Dark spikes or "hot pixels" have a corresponding rate of increase but, with a much higher dark current to begin with, can become quite dominant at CCD bakeout temperatures of +20 C. Although the analysis software tries to match dark frames of the appropriate temperature to the data being analyzed users should be alert for incorrect background subtraction during periods surrounding CCD bakeout. Dates of CCD bakeout can be obtained with the program PR_DATES_WARM and are listed in the appendix of the Reference Guide.

4.2.4 Artifacts in Optical Images from Radiation Damage

Areas of the CCD with high integrated X-ray dose, such as the east and west limbs, are observed to lose sensitivity for visible photons. The reason for this is still unknown. Thus, the aspect sensor images recorded before 14-Nov-92 when the entrance filter failed contain "ghost images" of the X-ray sun. The darkness of the ghosts fades with time to some degree.

For most uses of aspect images the ghosts have no effect. For quantitative studies with aspect images they may become important. Primitive flat-fielding routines are available. Hugh Hudson is the expert to consult.

4.2.5 SAA Effects on Images

The SXT operates through the South Atlantic Anomaly, for better continuity of coverage, even though the Yohkoh high energy sensors are switched off. SAA images are subject to lots of "hot pixels" and particle tracks from proton hits. These artifacts can be removed, to a fair degree, through use of the program DE_SPIKER.

4.2.6 Subtleties of Background Subtraction

In general, the background subtraction provided by SXT_PREP, DARK_SUB, and LEAK_SUB work amazingly well for such a complex problem. If background subtraction is a little off, substantial errors can accumulate in computing the intensity of large areas of faint emission. To better match exact exposure times the keyword */dc_interpolate* should be used. For cases where even this is not satisfactory, the keyword */shift_floor* will use the average of a 5×5 area in the lower left corner of the image as the background. This is usually only needed for the very shortest exposures.

Note that these routines leave the negative and zero values remaining from dark frame subtraction. These may need to be replaced with a positive value for, e.g., logarithmic display or ratio forming. By default SXT_TEEM will ignore negative intensity pixels when computing temperatures.

Dark subtraction will not remove cosmic or SAA artifacts which can be treated manually by replacing the offending pixel with the average of the surrounding pixels or through the use of DE_SPIKER.

After Nov-92, some background due to a visible light leak also needed to be removed. See section **??** for more details.

4.2.7 Charge Bleed-back

During fast transfer of a CCD image to reach the Region of Interest (ROI) of a PFI, charge builds up in the serial shift register of the CCD. This charge must be shifted out lest it bleed back onto the CCD and corrupt the image. A commandable guard band is provided to prevent this problem. However, on a few occasions charge bleed back is apparent in PFIs taken with the aspect sensor. The result is saturated columns appearing in the image, usually in the middle where 2 ROIs have been pasted together to create a 2 exposure PFI. A good (bad) example is

```
18-AUG-92  04:46:30  QT/H  NaBan/Open  Full Norm C  20   948.0  128x128
```

There is no way to recover data corrupted by bleed back.

4.2.8 CCD Pixelization

SXT has three on-chip summation modes available: full resolution (FR), half resolution (HR), and quarter resolution (QR). The pixel sizes are 2.45, 4.90, and 9.80 arcsec respectively. A factor to consider when working with images is the proper adjustments necessary when changing resolutions. The corner address saved in the index are the IDL CCD coordinates of the center of the binned pixel in the lower left corner.

Fig. **??** on page **??** shows some of the details of the CCD pixels, and how the pixels are summed on the CCD. Due to the camera design, the FR, HR and QR images are not perfectly aligned which each other. There is a shift of up to 3 full resolution pixels which needs to be accounted for when inter-comparing different resolution images.

There is also the age old question of whether to refer to the center of a pixel or to the corner of a pixel. We have decided to refer to the center of the pixel since it translates much better when working with fits between different resolutions.

See SXT Calibration Note 35 for a detailed discussion of the SXT CCD pixels and all of the various coordinate systems associated with the CCD: ground-based coordinate system using the camera system test set (CSTS), CCD readout pixel coordinate system, and others.

4.2.9 What is Really Zero Signal Level in Data Numbers (DN)?

The DN value passed out of the camera when there is no light incident on the CCD and the dark current generation is zero will not be 0 DN. The minimum level is set electronically to be slightly higher, plus the spurious charge during readout causes another offset. The following are the approximate DN levels for no light incident on the cooled CCD.

- Full Resolution Pixels = 13 DN

- Half Resolution Pixels = 30 DN
- Quarter Resolution Pixels = 69 DN

This means that if you have one raw image (which has not had the dark current image removed) with an average signal of 15 DN and another with 20 DN, that is not a 25% difference, it is over 300% different. This offset must be watched carefully when working with low signal levels, even after the dark image has been removed.

The above values are appropriate for data acquired prior to 13-Nov-92. After the entrance filter failure, all values increased 1–2 DN due to a change in the spurious charge. NOTE: A separate effect is that the dark current has been increasing gradually during the mission, and will continue to do so, which is caused by X-ray damage.

DARK_SUB (which is what SXT_PREP calls), will remove a single dark frame which is closest in exposure level to the input image. When removing that single dark image, it takes off the digital offset, plus the dark current (exposure dependent) portion. An even better method is to use the /DC_INTERPOLATE option, which will interpolate two dark images to correct for the exposure dependent dark current, and will also remove the digital offset.

4.3 The Mirror, Lens or Filters

4.3.1 Scattering by ND X-ray Filter

In order to extend the dynamic range of SXT for flare use, the forward filter wheel is equipped with a stainless steel mesh ("ND" filter) with a transmission of 0.0805 ± 0.0008. While the mesh causes no noticeable degradation of the image it has been found to scatter X-rays (SXT Calibration Note 34) at about the 0.7% level. This is a minor effect for the brightest features in a flare but can provide the dominant signal in nearby faint features. No adequate means for correcting for this effect has yet been derived. Therefore, for greatest accuracy it is presently advisable not to mix images with and without the ND filter in determining the T_e and EM of bright flare features and never to use ND filter images in the faint features. SXT_TEEM warns the user if the ND filter is included. E.g., the light curves, intensity, T_e , and EM of faint areas of ND flare images may be totally in error. Because the scattering is diffuse and smooth, the images themselves are quite adequate as pictures of the flares for morphological studies.

4.3.2 Point Spread Function

The point spread function (PSF) of the SXT has a narrow core and wide scattering wings. Laboratory measurements of the core of the PSF have been analyzed thoroughly by Martens (SXT Calibration Note 34). The shape of the PSF is well characterized by an elliptical Moffat function with a FWHM of about 1.5 CCD pixels (3.7 arcsec) over the central area (diameter = 470 pixels or 2300 arcsec) of the CCD. Between a radius of 1 and 10 CCD pixels the slope of the PSF falls off roughly as a power law of index -4.

There is as yet no released software for deconvolution of SXT images, although McTiernan has done some work on this using the maximum entropy method and Roumeliotis has used a modified Lucy method.

4.3.3 Mirror Scatter

The scattering wings of the SXT PSF begin to dominate the narrow core at about 20 arcsec from the center—at a level about 5 or 6 orders of magnitude down from the peak (see Fig. 4 in

the Tsuneta, *et al.* (1991 'Red Book'). The scattering wings may be characterized from over-exposed flares observed in FFI mode such as 6-Sep-92 18:48. Hara (to be published) has derived the following expression which describes the shape of the PSF wing for a flare of 6.9×10^6 K, through the thin filters

$$Wing(r, 6.9 \times 10^6) = 10^{-1.839} \times r^{-2.0} \qquad [r > 20'']$$

per full resolution SXT pixel and per unit intensity in the flare, with r specified in arcsec. The scattering properties of the mirror are wavelength dependent. This introduces a dependence upon input spectrum in correcting for the PSF scattering wings in data analysis. Hara represents this dependence in terms of a ratio of the mean wavelength of the flare and the mean wavelength of the reference (6.9×10^6 K) spectrum and gives the following expression for the PSF wing for other source temperatures.

$$Wing(r, T_e) = Wing(r, 6.9 \times 10^6) \times (L_{avg}(6.9 \times 10^6)/L_{avg}(T_e))$$

where L_{avg} is the average wavelength recorded by SXT through either the Al.1 or AlMg filters at temperature T_e.

Scattering wing corrections have not yet been derived for the thicker filters and programs for use of the preliminary algorithms derived by Hara have not yet been released for general use because of concerns of their applicability away from sun center.

4.3.4 Vignetting Correction

The SXT X-ray effective area varies across the 42×42 arcmin field-of-view. The effective area and response functions that are reported in other sections of this manual always refer to values for the optical axis of the telescope, where the effective area is maximum. The off-axis response has been measured during pre-launch calibration and has been refined with in-flight data. To a first approximation, the off-axis variation of effective area, or the vignette function, can be approximated by two non-concentric cones (see SXT Calibration Note 37). The inner- and outer-cones intersect one another at a radius of about 21 arcmin. Analysis of flight data indicates that the vignette function is actually more complicated and should at least be approximated by a cone with some flat distortions. These distortions were not detected in pre-launch calibration, and several questions about them remain. The vignette function is known to vary as a function of incident photon energy. Pre-launch measurements were made at three energies: 0.277 keV (C K), 1.49 keV (Al K), and 2.98 keV (Ag L). Measurements at the two lower energies gave results that were consistent with one another. Thus, we have characterized the SXT vignette functions as either "low" or "high" energy. The shape of the vignette function can be seen using the IDL routine HELP_VIGNETTE for which a sample plot is shown in Fig. **??**.

There are no fully approved routines to remove or correct for the SXT vignette function, however, there are a two preliminary routines. SXT_VIGNETTE will compute the vignette function as it is currently understood. The form and parameters of the shape may be changed as additional data and analysis become available. The routine SXT_OFF_AXIS will correct for the vignette function by calling SXT_VIGNETTE. Users are warned that these routines are preliminary and may not be the most appropriate technique to use, depending on the scientific application. However, they are certainly more accurate than no correction when intensities from different parts of the CCD must be compared.

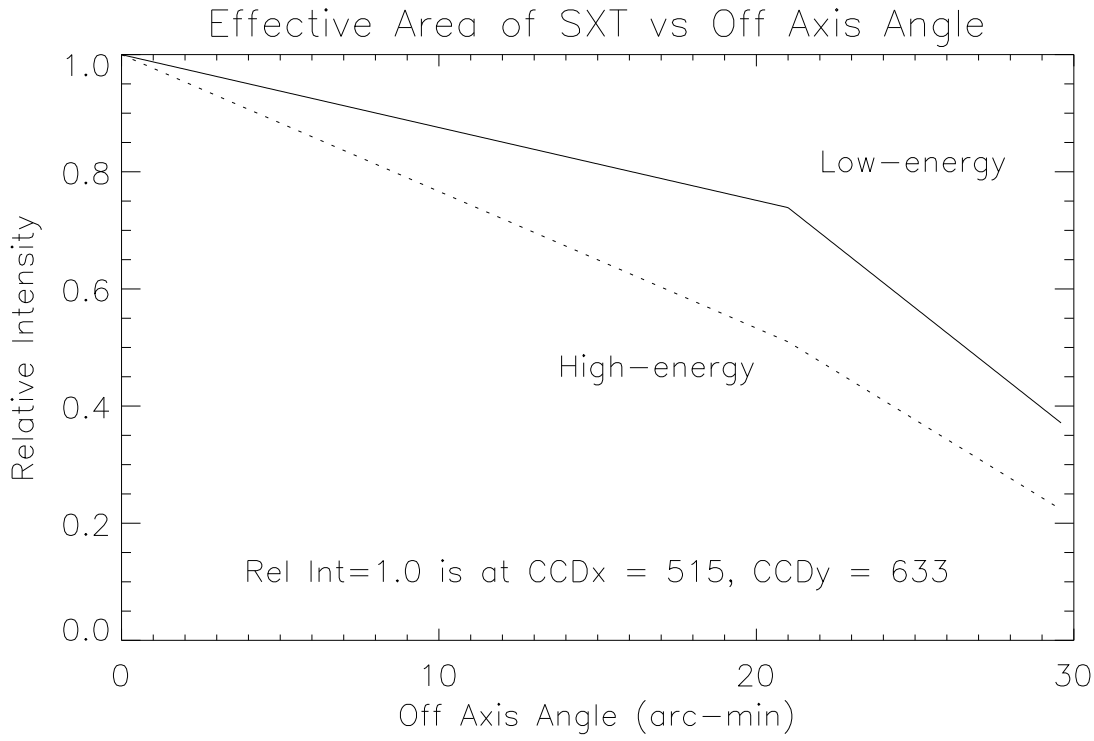

Figure 4.7: The effective area (or vignette function) as a function of off-axis angle. The solid curve was derived from C K and Al K data and the dashed curve from Ag L data.

4.3.5 Stray Visible Light

The SXT entrance filter consists of a small amount of titanium and aluminum deposited on Lexan. In order to guard against the possibilities of pinholes, two such filters were flown back-to-back with the Lexan surfaces facing each other. These filters cover the X-ray entrance annulus and are arranged as six back-to-back pairs, or twelve individual filters in all. On 29-Oct-92 between 04:30 and 06:30 UT it was noticed that the optical images contained an halo of diffuse light. On 13-Nov-92 at 16:50 UT the visible light images became completely saturated. It is now thought that in October 1992 one of the outer entrance filters broke either completely or partially. The resulting halo was produced by the light that leaked through the inner filter that was behind the broken outer filter. Once the outer filter failed, the inner filter had its Lexan surface exposed to solar UV radiation and after three weeks of continuous exposure, the Lexan material deteriorated, causing the filter to at least partially fail. The resulting hole in the entrance filter allows visible light to be reflected by the X-ray mirror into the focal plane.

From an analysis of the data acquired after 14-Nov-92 it has been calculated that the fraction of the open area is 0.0833. The SXT_FLUX and SXT_TEEM routines take this into account when computing the response functions. The effect is negligible for the thick filters and makes only a small effect for the thin filters, increasing the response slightly at longer wavelengths. No adequate explanation for the partial entrance filter failure has been determined. This value and the date are available from the routine GET_YO_DATES(/entrance,/verbose). Analysis and description of these artifacts are given in SXT Calibration Notes 38 and 39.

When the 8% transmission X-ray ND mask is used, the stray light intensity increases a

hundred fold. This is not as severe a problem as it sounds because exposures using the ND filter are generally quite short.

It has proven possible to acquire images with the SXT between 10 and 30 seconds before optical sunset—for which the atmosphere completely attenuates the X-ray sun with little effect on the visible illumination. These "terminator" images are routinely taken through all combinations of SXT filters for use in subtracting this stray light signal. This correction, along with dark frame subtraction, is provided by the program LEAK_SUB which will be updated from time to time as the terminator data base and correction algorithms improve. At present, LEAK_SUB is not perfect and over/under correction can be a problem you should be alert for. Because of complexity and partial randomness (especially for the thin Al filter), perfect straylight correction will never be possible.

4.4 Other Instrument and Operations Features

4.4.1 Data Compression

The CCD camera employs a 12-bit ADC but data are transferred to the DP (telemetry) as 8-bit numbers. For purposes of gain calibration and helioseismology it is important to maintain the full 12-bit accuracy. This is accomplished by commanding compressed data and the low-order 8 bits for the same region, and then restoring the full 12 bits (see the routine RESTORE_LOW8 described in the Reference Guide).

The compression of ADC numbers uses the following algorithm. Taking DN, or Data Number, to be the CCD digital camera output, and X the 8-bit compressed value, and M the 12-bit decompressed value,

- for DN ≤ 64

$$X(\mathrm{DN}) = \mathrm{DN}, M = X = \mathrm{DN}$$

- for DN > 64

$$X(\mathrm{DN}) = \mathrm{round}[59.249 + \sqrt{3510.39 - 9.50(431.14 - \mathrm{DN})}\,],$$
$$M = \mathrm{round}[0.10526X^2 - 12.473X + 431.14]\,.$$

These expressions are used by the routines SXT_DECOMP and SXT_COMP for decompression and compression, respectively.

The SXT compression algorithm is not lossless, and so the decompressed values, M, contain a small error due to decompression: $\delta M = |\mathrm{DN} - M|$. The algorithm has been selected so as to make the decompression error, δM, comparable to the statistical uncertainty. The decompression error is given by:

$$\delta M = 2 \times 0.10526X - 12.473\,,$$

which are optionally returned by the SXT_DECOMP routine.

4.4.2 Use of Low-8 Images in Optical Data

For X-ray images the error introduced by the SXT data compression is less than counting statistics so the compression from 12-bit (out of the CCD camera) to 8-bit numbers loses little

information. For aspect images the errors in counting statistics are far less than the data compression errors. In order to obtain the best statistical precision, the aspect images were often taken in both low-8-bit and compressed data modes separately. These are combined to provide full 12-bit precision through the use of the program RESTORE_LOW8. This procedure works best if the two exposures are close together in time to minizize the effects of spacecraft pointing drift and jitter.

4.4.3 Filter Alternation During AEC

The Automatic Exposure Control of the SXT is described in the "Red Book" and briefly in the Reference Guide. One aspect of the AEC algorithm is that if the image is overexposed, and the AEC software has reduced the exposure to the lowest exposure level possible, then the logic could insert a "thicker" filter to avoid saturation. This option is enabled or disabled by the sequence table. There has been confusion on occasion when the filter has changed for a given sequence "slot," even when there has been no table upload, or change in DP mode or DP rate. In most cases, the change in filter was due to AEC Filter Alternation.

The bottom line is that if exposure and ND filter adjustment do not suffice to maintain the desired exposure a thicker or thinner filter could be selected. Beware of this when analyzing flare data and an unexpected filter suddenly appears in the sequence!

4.4.4 The Roll Angle in the SXT Images

The azimuthal orientation of the SXT CCD is mis-aligned slightly with respect to the Yohkoh spacecraft. Thus, if the spacecraft is oriented so that the solar north direction is parallel to the "pitch" axis, in the SXT images solar north will not be exactly aligned with the y-axis of the CCD, but rotated a small amount counter clockwise. A useful routine for displaying a diagram of the roll angle relationships is HELP_ROLL. The precise roll angle was not measured prior to launch. The value has been determined from in-flight measurements and continues to be refined. It is approximately 1 degree. The value which is used currently in the on-line software can be checked by typing:

```
IDL> print,get_roll(/sxt)          ; Print SXT roll-angle (degrees)
```

When analyzing SXT images, one should be aware that the Yohkoh spacecraft roll orientation varies slightly. GET_ROLL by default returns the roll angle of SXT with respect to solar north, incorporating the CCD roll-angle and spacecraft roll angle. GET_ROLL tries to read the ATT database files if they are available (see the reference guide for more information). The ATT database already has the correction for seasonal variation that exists between the spacecraft's on-board definition and the true solar north value. If the ATT database is not available, the routine will return values based on a sinusoidal fit to the seasonal variations, but which does not take into account the true S/C roll.

4.4.5 Incorrect Location of Image Pieces in Some PFIs

Observing regions (OR) are composed of 64×64 PFI "blocks." The simplest observing region is 64×64, but quite often larger observing regions are used. For example, when the observing region is 256×192, there are 4 "blocks" in the E/W direction and 3 in the N/S. Because of the way that the SXT telemetry buffers work, it is necessary to take three separate exposures for a 256×192 observing region. The assembly of these "blocks" into an observing region is

performed properly for over 99% of the observing regions, however, there is a special case when a problem can occur.

When the telemetry mode is FFI dominant (the full frame images get the larger portion of the telemetry), it requires four major frames to telemeter a single 64×64 PFI "block". If any of the first portions of the "block" (which is 64×16) is missing, it will cause the image to be assembled incorrectly because of a lack of telemetry information. Be aware of occasional PFI portions which are not aligned properly.

4.4.6 Preparation of SFD images

SFD images are prepared from long and short exposure FFIs to extend the dynamic range of a given image to about 1×10^6. The program MK_SFD is used for this purpose. These images are used to make the SXT "movie" and are especially valuable for surveying the data archive. Users should recognize that the SFD images are automatically prepared on a production line basis as part of the data reformatting process and should be alert for artifacts and features which are not of solar origin. Also, some areas of the images will have smoothed data inserted to replace saturation-bleed regions.

While, in general the SFD data are quantitatively correct, quantitative analysis should generally resort to the original SFR files which, for a variety of reasons, will often have images which are not made into SFD images. Users wishing to make their own composite images from 2 or 3 images of different exposure are referred to the program SXT_COMPOSITE.

4.5 Contact Persons

If you have any question about SXT software and/or instrument, or if you need any advice in SXT data analyses, contact:

`yla@solar.physics.montana.edu`

4.6 References

- Tsuneta, S., Acton, L., Bruner, M., Lemen, J., Brown, W., Caravalho, R., Catura, R., Freeland, S., Jurcevich, B., Morrison, M., Ogawara, Y., Hirayama, T., and Owens, J., Solar Phys. 136, 37-67 (1991), "Red Book."
- Lemen, J. R., "SXT X-Ray Effective Area," SXT Calibration Note 31, (Rev. A, 1993).
- Martens, P. C., "White Sands Measurements of the Point Spread Function," SXT Calibration Note 34, (Rev. A, 1993).
- Morrison, M., "SXT CCD Pixel Description," SXT Calibration Note 35, (Rev. A, 1993).
- Fuller, R. A., and Lemen, J. R., "SXT X-Ray and Optical Axes," SXT Calibration Note 36, (Rev. A, 1994).
- Fuller, R. A., Lemen, J. R., and Acton, L. W., "SXT X-Ray Vignetting Function," SXT Calibration Note 37, (Rev. A, 1994).
- Acton, L. W., "Origin of Thin Aluminum Straylight Features," SXT Calibration Note 38, (Rev. C, 1993).
- Acton, L. W., "Analysis of Thin Aluminum Sunset Straylight Images," SXT Calibration Note 39, (Rev. B, 1993).

5 Wide Band Spectrometer (WBS)

5.1 Basic Instrument Characteristics

WBS has spectroscopic capabilities in a wide energy band from soft X-rays to gamma-rays. It consists of a soft X-ray spectrometer (SXS), hard X-ray spectrometer (HXS), gamma-ray spectrometer (GRS), and radiation belt monitor (RBM). Of these, SXS, HXS, and GRS aim at solar flare observations, but RBM serves to sound the alarm for radiation belt passage. All of these detectors have pulse count (PC) data and pulse height (PH) data. PC is the sum of all counts for a given energy range, and PH is essentially an energy loss spectrum as a function of energy. Brief instrument descriptions of SXS, HXS, and GRS are given here. Detailed descriptions can be found in Yoshimori *et al.*, (1991).

5.2 Soft X-Ray Spectrometer (SXS)

SXS consists of two gas proportional counters (SXS-1 and SXS-2) filled with xenon and carbon dioxide (1.16 atm) and has a beryllium window of 0.15 mm thickness. The field of view of each detector is 10 deg x 10 deg. Each of the two detectors covers the photon energy band from 3 keV to 40 keV. SXS-1 has a large effective area which is suitable for detection of small flares, whereas SXS-2 has a small effective area which is suitable for detection of large flares. The energy resolution is about 20 % at 5.9 keV and 12 % at 22 keV. The inflight energy calibration is achieved by detection of 5.9 keV line emitted by a Fe-55 radioactive source. Both SXS-1 and SXS-2 have two PC channels; PC11 and PC12 for SXS-1, and PC21 and PC22 for SXS-2. The first suffix denotes the counter and the latter suffix indicates the energy channels (low; 1 and high; 2). For example, PC12 is the higher energy band of SXS-1. The lower energy bands range from LD to MD1, while the higher energy bands range from MD1 to MD2. These discrimination levels (LD, MD1, and MD2) as well as the gains of the pulse counting electronics circuit (h) and the high tension levels (g) can be independently selected among the four-entry options, respectively.

The discrimination level (y=LD, MD1, and MD2) of the SXS PC channels can be obtained by the following relations.

```
y(keV) = a * (x +9)/h/g
SXS-1 :  a = 0.30
```

	h	g	LD(x)	MD1(x)	MD2(x)
00	1.00	1.00	0	40	103
01	0.67	1.36	0	58	127
10	1.47	1.75	0	74	127
11	2.24	2.75	0	91	127

```
SXS-2 :  a = 0.28
```

	h	g	LD(x)	MD1(x)	MD2(x)
00	1.00	1.00	0	36	94
01	0.66	1.47	0	54	127
10	1.47	1.87	0	69	127
11	2.15	3.02	0	85	127

The settings were all null (00) before June 18, 1992 and only the gains were changed to g = 01 (for SXS-1 and SXS-2) since then.

The total deadtime of these PC channels is 9 μs. The correction factor is tabulated in the file $DIR_WBS_CAL/dtcorrf.dat.

Distortion of the energy versus pulse-height relationship in the PH mode was found after the launch, which might have resulted from the failure of the pulse-height-analysis electronics circuit. No reliable energy calibration for the PH data is available at the moment.

5.3 Hard X-Ray Spectrometer (HXS)

HXS consists of a NaI(Tl) scintillator (7.6 cm in diameter and 2.5 cm in thickness). The window of NaI scintillator is covered with two kinds of stainless steel absorbers of 13.8 cm^2 × 0.08 mm thickness and 31.8 cm^2 × 1 mm thickness to suppress low-energy X-rays associated with solar flares.

HXS covers the photon energy band from 20 keV to 650 keV (1991 Oct. 1 – 1992 June 9) and from 24 keV to 830 keV (1992 June 9 – present). The energy resolution is 26 % at 22 keV and 13 % at 88 keV. Inflight energy calibration is achieved by detection of the 60 keV line emitted by an Am-241 radioactive source. In addition, the 191 keV line emitted by radioactive I-123 and the 511 keV line emitted by positron annihilation are used for inflight energy calibration.

HXS has two PC channels PC1 and PC2, and a 128-channel PH. The energy bands of PC1, PC2 and PH are given in the table in section **??**.

The HXS instrument calibrations are stored in the following data files located in the directory $DIR_WBS_CAL (/ys/wbs/response) and in IDL programs.

File	*Contents*
hxs_01.rel hxs_21.rel	*Channel number vs. energy relation* (9-Jun-92 – present) (1-Oct-91 – 9-Jun-92) HXS amplification gain was changed on 9 June,1992.
hxs_conv260.rel	*Table of 260 incident photon energies* for the 260 x 32 response matrices (hxs_01_conv260.resp and hxs_21_conv260.resp)
hxs_01_conv260.resp hxs_21_conv260.resp	*HXS response matrix (260 rows x 32 columns)* (9-Jun-92 – present) (1-Oct-91 – 9-Jun-92)
dtcf_pc_hxs.pro	Deadtime correction factor for HXS-PC
dtcf_ph_hxs.pro	Deadtime correction factor for HXS-PH

5.4 Gamma-Ray Spectrometer (GRS)

GRS consists of two identical BGO (bismuth germanate oxide) scintillators (GRS-1 and GRS-2). Each scintillator is 7.6 cm in diameter and 5.1 cm in thickness. The window of each BGO scintillator is covered with a 0.5 mm thick lead absorber to suppress low-energy gamma-rays associated with solar flares. GRS covers the photon energy band from 0.3 MeV to 100 MeV. The energy resolutions is 14 % at 0.662 MeV and 6 % at 4.07 MeV. Inflight energy calibration is achieved by detection of the 1.173 and 1.333 MeV lines emitted by a Co-60 radioactive source. Each GRS has a six-channel PC, a 128-channel PHL and a 16-channel PHH. The energy bands of the PC and PH are given in the table in section **??**.

The GRS instrument calibration are stored in the following data files located in the directory $DIR_WBS_CAL (/ys/wbs/response) and in IDL programs.

File	*Contents*
grs1_40.rel	Channel number vs. energy relation for GRS-1
grs2_40.rel	Channel number vs. energy relation for GRS-2
grs1_40_conv260.rel	Table of 260 incident energies for the 260 x 128 response matrix grs1_40_conv260.resp
grs2_40_conv260.rel	Table of 260 incident energies for the 260 x 128 response matrix grs2_40_conv260.resp
grs1_40_conv260.resp	GRS-1 response matrix (260 rows x 128 columns)
grs2_40_conv260.resp	GRS-2 response matrix (260 rows x 128 columns)
dtcf_ph_grs1l.pro	Deadtime correction factor for GRS-PHL1
dtcf_ph_grs2l.pro	Deadtime correction factor for GRS-PHL2

5.5 WBS Output Data

Primary data output of SXS, HXS and, GRS are pulse count (PC) data and pulse height (PH) data. The PC and PH data provide the counting rate time profiles and energy loss spectra, respectively. Each of SXS produces two PC data every 0.25 s (2 s) and a 128-channel PH spectrum every 2 s (16 s) in a high (medium) bit rate mode. HXS produces two PC data every 0.125 s (1 s) and a 32-channel PH spectrum every 1 s (8 s) in the high (medium) bit rate mode. Each of GRS produces six PC data every (0.25 and 0.5 s) and 128-channel PH data every 4 s (32 s) in the high (medium) bit rate mode. The data output of SXS, HXS, GRS and RBM are summarized in the following table.

WBS Data		Time Resolution High bit rate	Medium bit rate
SXS-1	PC11 (3-15keV*)	0.25 s	2 s
	PC12 (15-40keV*)	0.25 s	2 s
SXS-PH1	128 ch (3 - 30 keV*)	2 s	16 s
SXS-2	PC21 (3-15keV*)	0.25 s	2 s
	PC22 (15-40keV*)	0.25 s	2 s
SXS-PH2	128 ch (3 - 30 keV*)	2 s	16 s
*The values of energies given above are nominal.			
(1991 Oct.1-1992 June 9)			
	HXS-PC1 (20-65keV)	0.125 s	1 s
	HXS-PC2 (65-657keV)	0.125 s	1 s
	HXS-PH 32 ch (20 - 657 keV)	1 s	8 s
(1992 June 9 - present)			
	HXS-PC1 (25-75keV)	0.125 s	1 s
	HXS-PC2 (75-830keV)	0.125 s	1 s
	HXS-PH 32 ch (25 - 830 keV)	1 s	8 s
GRS-1	PC11 (0.27-1.04MeV)	0.25 s	2 s
	PC12 (1.04-5.47MeV)	0.25 s	2 s
	PC13 (5.47-9.3MeV)	0.5 s	4 s
	PC14 (9.3-13.1MeV)	0.5 s	4 s
	PC15 (8-30MeV)	0.5 s	4 s
	PC16 (30-100MeV)	0.5 s	4 s
GRS-PHL1	128ch (0.3-13.1MeV)	4 s	32 s
GRS-PHH1	16 ch (8 - 100 MeV)	4 s	32 s
GRS-2	PC21 (0.3-1.24MeV)	0.25 s	2 s
	PC22 (1.24-5.66MeV)	0.25 s	2 s
	PC23 (5.66-9.37MeV)	0.5 s	4 s
	PC24 (9.37-13.68MeV)	0.5 s	4 s
	PC25 (8-30MeV)	0.5 s	4 s
	PC26 (30-100MeV)	0.5 s	4 s
GRS-PHL2	128ch (0.3-13.6MeV)	4 s	32 s
GRS-PHH2	16 ch (8 - 100 MeV)	4 s	32 s
RBM-SC-PC1	(5 - 50 keV)	0.25 s	2 s
RBM-SC-PC2	(50- 300 keV)	0.25 s	2 s
RBM-PH	32 ch (5 - 300 keV)	1 s	8 s
RBM-SSD	(>20 keV)	0.25 s	2 s

5.6 Contact Persons

If you have any question about WBS software and/or instrument, or if you need any advice in WBS data analyses, contact:

yosimori@ax251.rikkyo.ac.jp (Yoshimori)
x024862@jpnrky00.bitnet (Yoshimori)
ohki@flare2.solar.isas.ac.jp
watanabe@uvlab.mtk.nao.ac.jp

5.7 References

- Yoshimori, M., Okudaira, K., Hirasima, Y., Igarashi, T., Akasaka, M., Takai, Y., Morimoto, K., Watanabe, T., Ohki, K., Nishimura, J., Yamagami, T., Ogawara, Y., and Kondo, I., Solar Phys. 136, 69-88 (1991).

6 Spacecraft Attitude, Ephemeris and Coordinate Systems

6.1 Spacecraft Attitude Control System (ACS)

The attitude control system uses momentum wheels, magnetic torquers, and control-moment gyros as the actuators. As the attitude sensors, two sun sensors and a star tracker, as well as geomagnetic sensors, are available for determining the spacecraft pointing relative to the direction of the sun and to the ecliptic plane, respectfully. An inertial reference unit comprising four gyros detects changes of attitude with time. HXA??

6.1.1 Inertial Reference Unit (IRU)

Four gyros are present on the Yohkoh spacecraft, one each in X, Y and Z and the fourth one in a 45 degree skew position. The IRU values are used by the IDL software to create the attitude (ATT) database.

6.1.2 Two-dimensional Fine Sun Sensor (TFSS)

More...

6.1.3 Star Tracker (STT)

Used to define spacecraft roll. Tracks star Canopus. Eclipses...

6.1.4 Geomagnetic Sensors (GAS)

What are these??

6.1.5 HXT Aspect Sensor (HXA)

The HXT aspect sensor (HXA) consists of two 1-dimensional CCD arrays located in a cross, 90 degrees to each other. The cross is rotated approximately 45 degrees relative to the SXT and HXT coordinate system. The HXA values are used by the IDL software which creates the attitude (ATT) database. There are fiducial marks which can reduce the resolution of the HXA results if the limb coincides with the fiducial mark.

6.1.6 Attitude Determination Software (ADS)

The attitude determination software (ADS) runs on the FACOM mainframe at ISAS and has been found to have noise problems (probably due to the TFSS). The ATT IDL database was created to replace the ADS results, which uses the HXA and IRU raw data. The ATT database does copy the ADS roll results into the database.

6.2 ACS Performance

6.2.1 Pointing Accuracy

Table of values

6.2.2 Spacecraft Jitter

Due for movement of filter wheel.

6.2.3 Sensor Problems

In Sep-93, it was decided to switch to the X, Y and skew gyros (instead of X, Y, and Z) because of the high drift rate of the Y gyro. Stil believed to be functional??

The two dimensional fine sun sensor had a noise problem shortly after launch and it's usefulness was greatly reduced.

Loss of spacecraft Roll... See appendix ?? for list of dates...

6.3 Instrument and Spacecraft Co-alignment

Summery of paper by Wuelser et al. (1998)

6.4 Spacecraft Ephemeris

Ranging. ORB and FEM files.

6.5 Contact Persons

If you have any question about spacecraft attitude, ephemeris and coordinate systems, contact:

`yla@solar.physics.montana.edu`

6.6 References

- The "Red" Book: "The Yohkoh (Solar-A) Mission", Solar Physics, Volume 136, No.1 1991.
- The 'Blue' Book: Solar-A (M-3SII-6) Engineering Reference Book (written in Japanese).
- Wulser,J.-P., Hudson,H.S., Nishio,M., Kosugi,T., Masuda,S, and Morrison,M., "Precise Determination of the Coordinate Systems for the YOHKOH Telescopes and the Application of a Transit of Mercury", 1998, Solar Physics, v.180, p.131-156

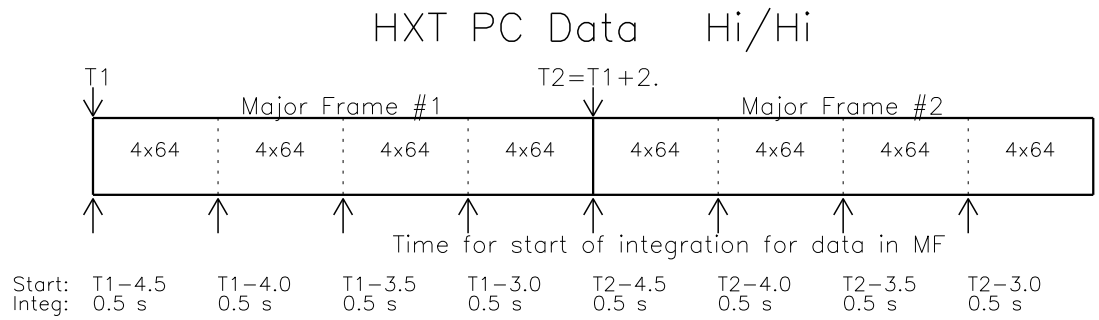

Figure A.8: Timing of HXT data for Hi/Hi telemetry frames

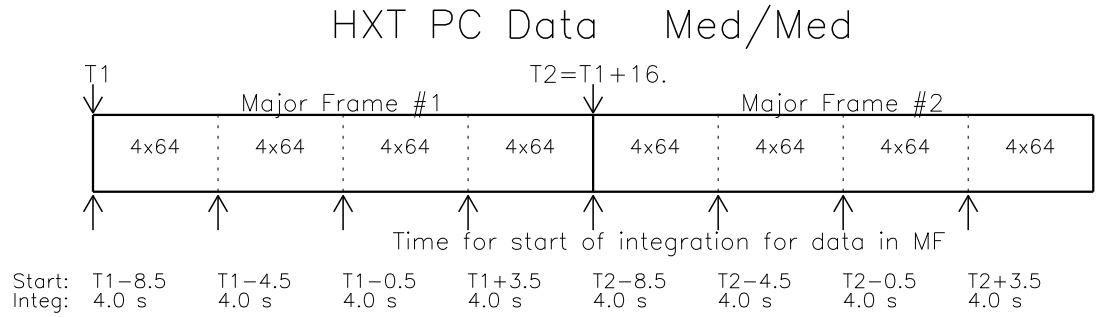

Figure A.9: Timing of HXT data for Med/Med telemetry frames

A Details on the Time Tags on the Data

A.1 Bragg Crystal Spectrometer (BCS)

Details for the BCS time tags were not available at the time of publication.

A.2 Hard X-Ray Telescope (HXT)

The HXT data is "pre-stored" in a buffer before being inserted into the telemetry. This pre-storage generally results in a 4.5 sec offset in the time saved in the index for high telemetry rate data, and 8.5 sec offset for medium telemetry data. See Figures **??** through **??** for a diagram of the timings. Unfortunately, not all programs correct for this offset when displaying the data. The user should look at the source code or send a message to the author asking for details.

HXT data are delayed by an additional 62.5 ms in the telemetry buffer in DP (see e.g. pp. 68-69 of the 'Blue Book'). Suppose Tf is a time tag which is attached to a certain telemetry frame, then the corresponding time tag T0 for HXT is: T0 = Tf-62.5 ms. To be precise, labels T1 and T2 in the HXT timing Figure **??** through **??** correspond to T0, rather than Tf.

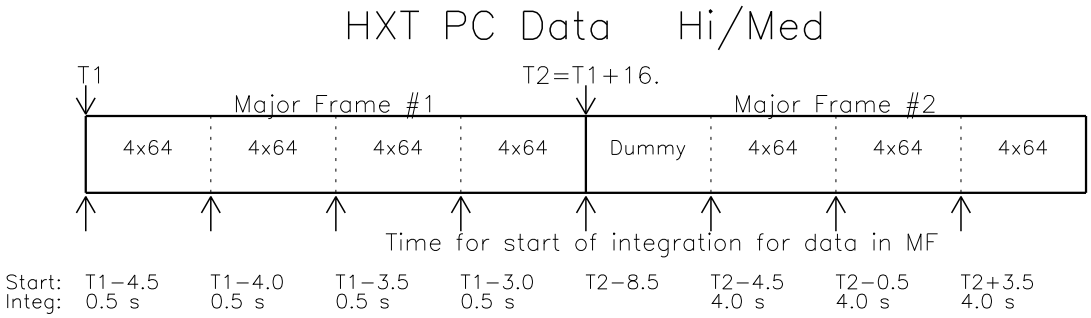

Figure A.10: Timing of HXT data for Hi/Med telemetry frames

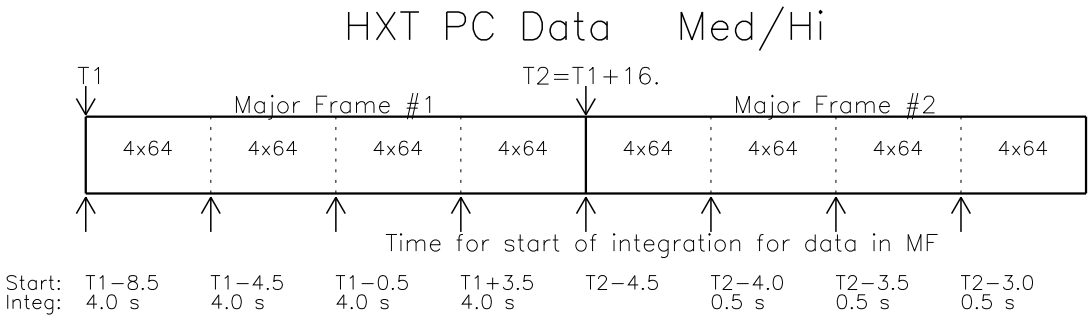

Figure A.11: Timing of HXT data for Med/Hi telemetry frames

NOTE: T2 is not necessarily T2=T1+16.0 for the case of MED to HI telemetry rate change. It is 16.0 sec only when a QUICK-HI transition for invoking flare-mode does not take place at the boundary of medium-bit rate major frames. Even if T2=T1+16.0, there is a data gap between the end of MED major frame and the beginning of HI major frame (i.e. T1+7.5 not equal to T2 − 4.5).

A.3 Soft X-Ray Telescope (SXT)

Figure **??** shows the delay in the time tags for the SXT images. There is a delay between the major frame time and the time that SXTE-J triggers an exposure (exposures are taken on the major frame boundaries). The SXTE-J delay is included in the time saved in the index. The delay in the SXTE-U between receiving the exposure trigger and the actual start of integration is not included in the time in the index. The user must get the exposure latency from the GT_EXPLAT routine, whose values typically range from 50 to 100 millisec.

The first example below shows how to get the true start of integration time of an image. The second example shows how to get the mid point of the integration time.

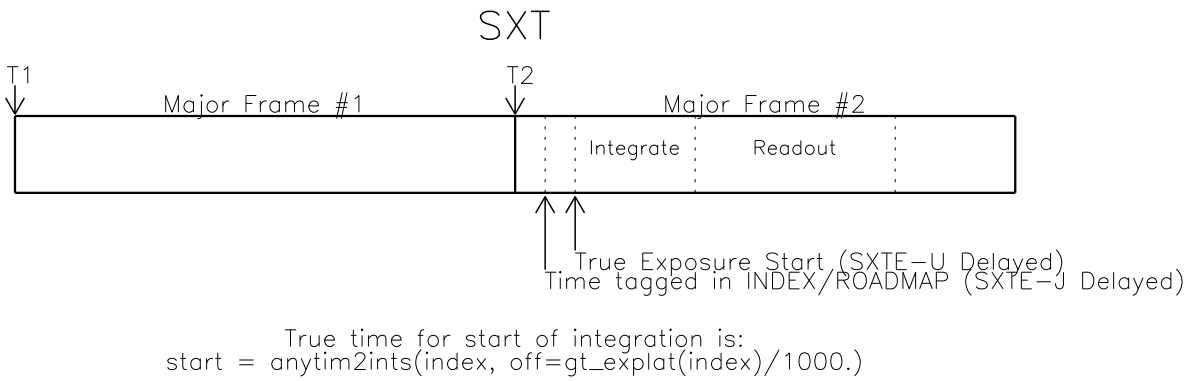

Figure A.12: Timing of SXT data

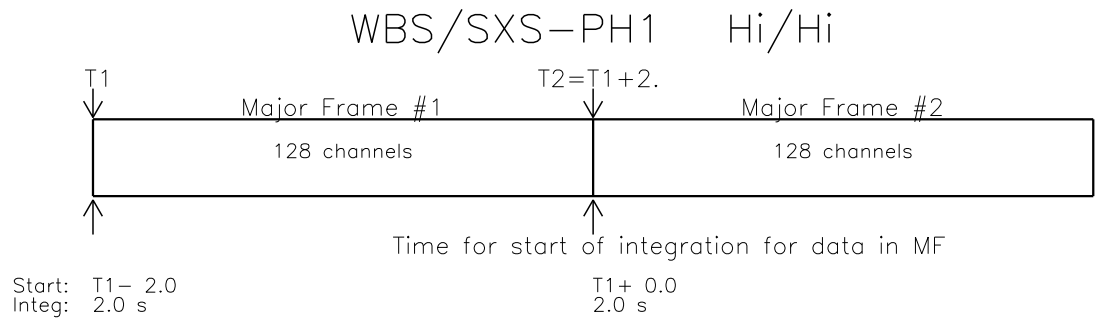

Figure A.13: Timing of WBS SXS-PH data

IDL> **start = anytim2ints(index, off=gt_explat(index)/1000.)**
IDL> **mid = start + gt_expdur(index)/1000./2.)**

A.4 Wide Band Spectrometer (WBS)

Figures **??** through **??** show some examples of the WBS timing. It takes two major frames to assemble a full set of WBS data. In most cases, multiple repeats of a spectra are saved during those two major frames. Details of the WBS time tags during telemetry rate changes were not available at the time of publication.

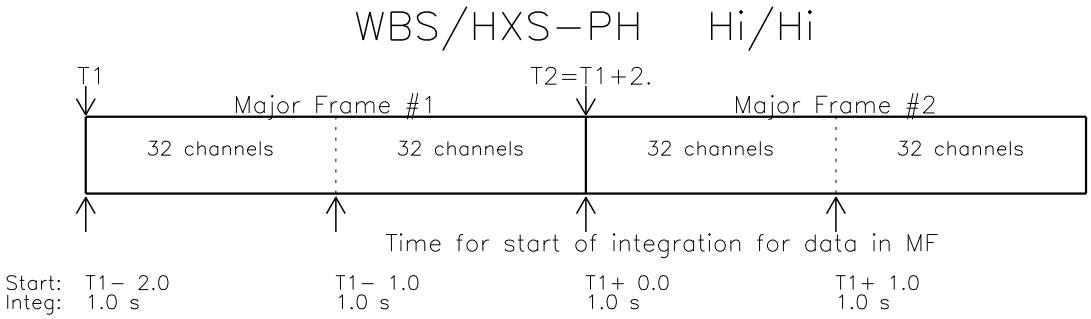

Figure A.14: Timing of WBS HXS-PH data

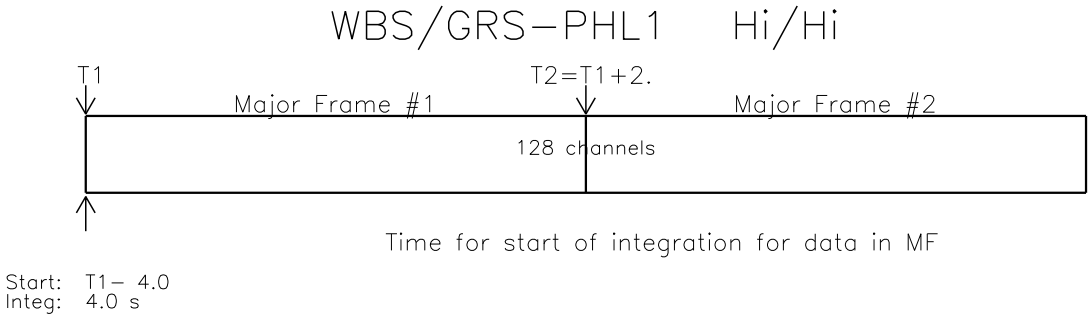

Figure A.15: Timing of WBS GRS-PHL data

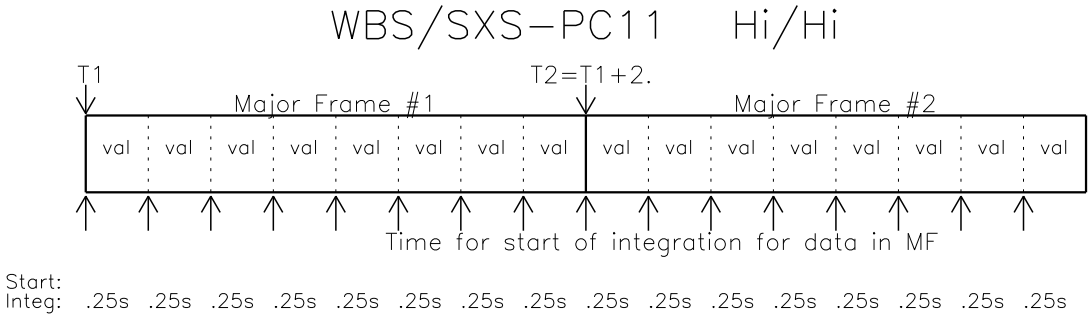

Figure A.16: Timing of WBS SXS-PC data

B Details of the SXT CCD Pixels

Fig. **??** shows the SXT CCD. The orientation of the CCD in the figure corresponds to the standard display in IDL in which full-Sun images have Solar-North at the top and East at the left. There is a coordinate system in the figure which is referred to as "IDL" coordinates, with IDL(0,0) corresponding to the lower left corner (which is nearest the south-east portion of the solar image). The physical read-out of the CCD occurs from North to South (top to bottom) as a parallel transfer into the serial register and then is read out from east to west (or from left to right in the figure). The physical device coordinate system in the figure is referred to as the "CCD" coordinate system. CCD(0,0) is in the lower right corner (which is nearest the south-west portion of the solar image). Note that CCD(1,0) = IDL(1023,0). This transformation is made automatically by the reformatter (i.e., YODAT returns images already converted to IDL coordinates). Also note that the column corresponding to CCD(0,*) is not included in telemetry. In fact, the on-chip summing is not exactly registered between full-, half-, and quarter- resolution modes. For example, in quarter-resolution, one would expect IDL_Q(0,*) to correspond to in full-resolution IDL_F(0:3,*), but instead it corresponds to IDL_F(3:6,*). For this reason, a simple REBIN or CONGRID function to convert SXT images to a higher or lower resolution will result in a slight mis-alignment. The GT_CORNER and GT_CENTER routines apply the correct shifts corresponding to the various image resolution modes. SXT Calibration Note 35 contains more details about the SXT pixel coordinate system.

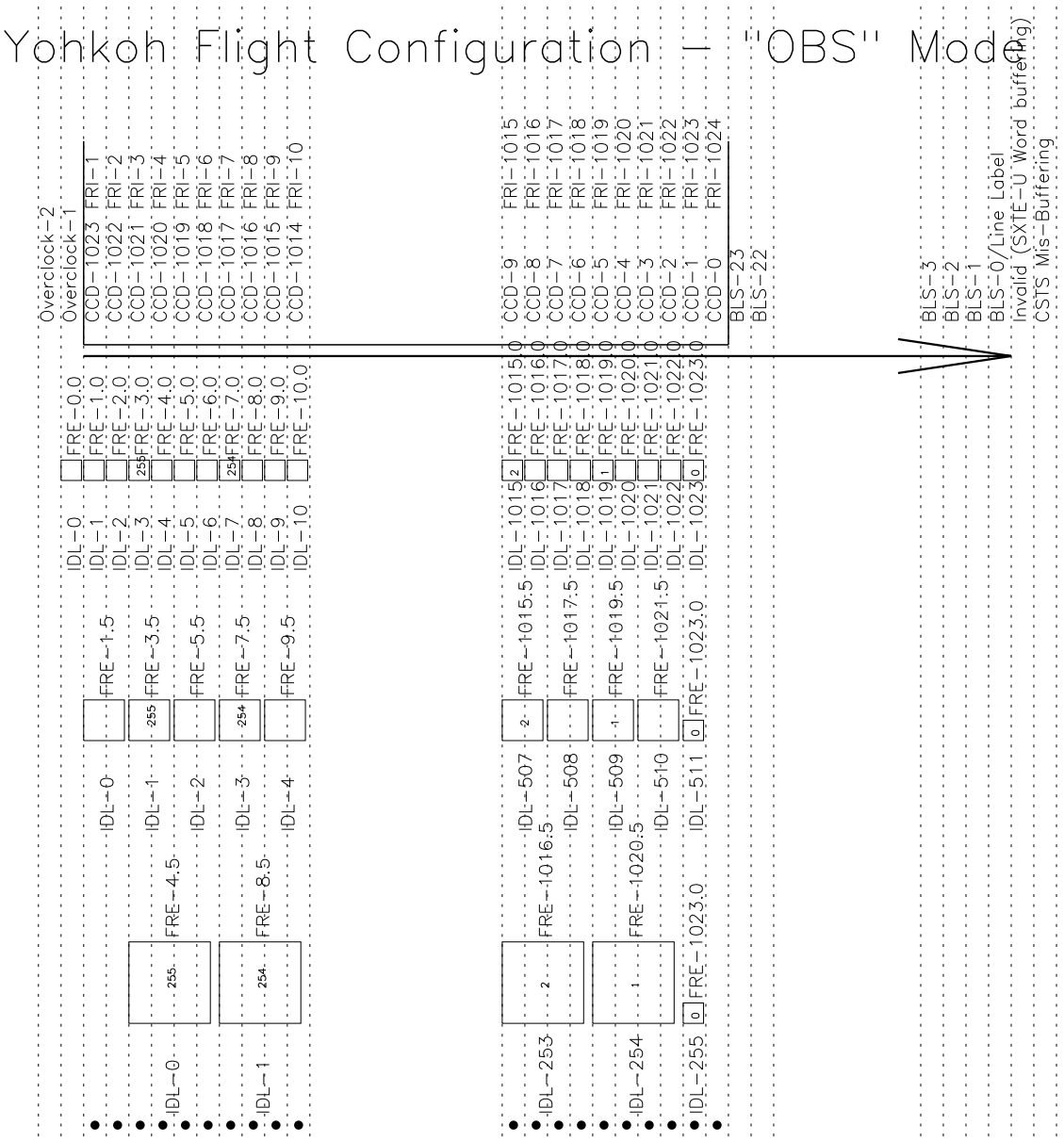

Figure B.17: SXT CCD Pixel Layout

C Dates of Significant SXT Activities

C.1 Dates that SXT CCD was Baked Out

The following table shows the dates that the SXT CCD thermo electric cooler (TEC) was turned off, and the TEC heater was turned on. The routine PR_DATES_WARM can generate this list at any time for sites which have the SSL database.

```
PR_DATES_WARM Program Run: 11-Jan-1994 22:51:01.00

   Date          Date           Approx #      High
   Warm          Cold          days warm      Temp
```

```
 9-JAN-92     10-JAN-92       2 days at   -0.6 C
 8-APR-92     11-APR-92       4 days at   23.8 C
 9-JUN-92     11-JUN-92       3 days at   -2.5 C
 4-SEP-92      6-SEP-92       3 days at   -1.2 C
 8-JAN-93      9-JAN-93       2 days at   23.8 C
21-JAN-93     22-JAN-93       2 days at   23.8 C
 5-APR-93      6-APR-93       2 days at   23.8 C
 4-JUL-93      5-JUL-93       2 days at   22.5 C
22-AUG-93     24-AUG-93       3 days at   25.2 C
 8-NOV-93     10-NOV-93       3 days at   23.8 C
```

C.2 Table of Number of SXT Images and Dark Current Levels

```
PROGRESS_SUMMARY.PRO  Ver 2.2 12-Aug-93
Program Run: 11-Jan-1994 23:21:16.00
```

Month	Full Frame Images		Observing Region Images				
	Received	Lost	Received			Lost	Loss %
			QT	FL	Tot		
Sep-91	517	397	21174	3541	24715	5481	18.15
Oct-91	4106	2532	6393	12437	18830	3401	15.30
Nov-91	5291	2475	12149	14696	26845	10952	28.98
Dec-91	4858	3228	4983	16837	21820	6910	24.05
Jan-92	5544	3177	10084	5972	16056	6849	29.90
Feb-92	5305	2803	16932	11382	28314	12019	29.80
Mar-92	6248	2361	20367	2653	23020	9458	29.12
Apr-92	6734	3500	20094	5423	25517	12390	32.69
May-92	7032	3158	25464	4589	30053	13745	31.38
Jun-92	6937	3112	23307	13221	36528	12627	25.69
Jul-92	6345	3275	23941	10510	34451	14717	29.93
Aug-92	6572	2978	24207	11154	35361	13550	27.70
Sep-92	6087	2916	26832	20042	46874	15729	25.12
Oct-92	6743	2589	50985	14709	65694	23687	26.50
Nov-92	6658	2939	24416	14696	39112	12924	24.84
Dec-92	6775	2999	24253	6633	30886	12356	28.57
Jan-93	6888	3351	24067	4861	28928	13069	31.12
Feb-93	6833	3004	24479	18149	42628	12302	22.40
Mar-93	7177	3460	25874	19537	45411	14657	24.40
Apr-93	7754	3644	34128	8352	42480	17967	29.72
May-93	8571	3950	41832	7518	49350	21971	30.81
Jun-93	7340	2589	64545	12539	77084	26299	25.44
Jul-93	8259	3650	47561	5352	52913	24213	31.39
Aug-93	7628	3638	30705	3563	34268	17436	33.72
Sep-93	6875	2899	22697	5600	28297	11252	28.45
Oct-93	7474	3657	33782	7548	41330	20104	32.72
Nov-93	8353	4015	42180	5849	48029	24669	33.93
Dec-93	5143	2777	17806	8640	26446	11503	30.31
Jan-94	0	0	0	0	0	0	30.31
Total	180047	85073	745237	276003	1021240	402237	28.26

```
Number of Full Frame Images Received:              180047
```

Number of Observing Region Images Received: 1021240
Total: 1201287

Approximate Number of Shutter Moves/CCD Readouts: 2128671

NOTES: * The loss of images is mainly due to BDR overwrites, but there are also occasional DSN dumps which are lost.
* It is common to have observing regions which contain more than 64 lines, which requires multiple exposures to make a single observing region image. This is why the number of shutter moves is larger than the number of images received plus those lost.

Month	Avg Dark Level (DN)	Avg Dark Level (e/sec)	# of Dark Spikes Over 48	# of Dark Spikes Over 64	CCD Warmings High / # Temp /Days	Front Support Temp	Optical Trans (%)
Oct-91	31.07	21.3	509	261		10.5	77.8
Nov-91	31.06	20.9	648	277		11.9	64.4
Dec-91	31.04	20.2	804	353		14.0	52.5
Jan-92	31.13	23.6	985	450	0.5 / 2	14.9	38.4
Feb-92	31.32	30.8	1176	544		14.3	31.7
Mar-92	31.47	36.5	1355	626		14.8	25.1
Apr-92	31.44	35.2	1323	610	23.8 / 4	14.6	22.8
May-92	31.65	43.1	1417	653		14.4	20.1
Jun-92	32.12	60.9	2215	880	-2.5 / 3	15.1	17.4
Jul-92	32.22	64.4	1852	832		15.5	14.1
Aug-92	32.21	64.1	1922	886		14.9	13.1
Sep-92	32.38	70.5	2062	954	-1.2 / 3	15.9	12.2
Oct-92	32.64	80.3	2317	1055		16.8	11.5
Nov-92	36.24	215.1	6112	1391		18.0	11.0
Dec-92	42.58	452.8	17390	2024		17.9	N/A
Jan-93	42.59	453.1	13006	2034	23.8 / 2	19.2	N/A
Feb-93	42.28	441.5	13895	2090		17.7	N/A
Mar-93	43.14	473.8	14047	2151		17.7	N/A
Apr-93	43.13	473.4	14304	2146	23.8 / 2	16.9	N/A
May-93	43.45	485.3	16405	2357		17.3	N/A
Jun-93	44.03	507.2	20037	2531		16.3	N/A
Jul-93	44.52	525.6	23977	2700	22.5 / 2	17.7	N/A
Aug-93	44.24	515.0	21879	2643	25.2 / 3	17.2	N/A
Sep-93	45.07	546.2	27469	2745		17.5	N/A
Oct-93	45.40	558.6	31684	2982		17.7	N/A
Nov-93	45.31	554.9	31892	3224	23.8 / 3	19.7	N/A
Dec-93	45.86	575.7	37517	3057		19.0	N/A
Jan-94	N/A	N/A	N/A	N/A		0.0	N/A

NOTES: * The dark current calculations are using full half resolution 2.668 sec

```
   images not taken in during the SAA.  The dark current rate assumes a
   "fat zero" of 30.5 DN and a gain of 100 e/DN.
 * The entrance filter failure of 13-Nov-92 eliminated the capability of
   taking optical images, so the optical transmission is not available
   after Nov-92.  It also caused an increase in the dark current signal,
   however some of the increase shown here is an increase in the readout
   noise and is not a function of exposure duration.
```

C.3 Dates of SXT Entrance Filter Failures

Now been several...

Include IDL command to list them.

D Attitude Control System (ACS) Related Items

D.1 Dates When Yohkoh was at non-zero Roll

Mostly until they realized that you had to set the STT timer... This is late 1991, early 1992.

E Miscellaneous Yohkoh Information

E.1 Amount of Yohkoh Data per Week

WEEK_TOTALS.PRO Ver 2.0 11-Jan-93
Program Run: 11-Jan-1994 22:48:05.00

		Number of Megabytes of Data for each Week								
Week	#Fil	ADA	BDA	CBA	HDA	SFR	SPR	WDA	Totals All	Totals No-CBA
91_37	64	17.2	4.4	57.9	4.7	15.2	9.6	8.3	117.2	59.3
91_38	63	28.1	4.8	94.5	8.7	44.4	71.0	27.8	279.3	184.8
91_39	74	30.9	31.1	105.9	28.7	58.7	97.0	44.2	396.4	290.5
91_40	54	24.2	27.9	83.9	14.3	100.5	34.1	35.5	320.3	236.4
91_41	68	29.5	29.1	100.1	15.3	131.4	48.5	43.4	397.3	297.2
91_42	61	21.4	17.3	78.1	8.6	79.1	22.2	22.8	249.4	171.3
91_43	68	25.4	21.6	88.2	18.1	88.1	42.4	31.9	315.7	227.5
91_44	82	34.0	26.2	116.5	25.2	154.7	67.9	48.1	472.6	356.1
91_45	101	41.2	24.8	143.2	24.1	204.3	69.7	55.9	563.1	419.9
91_46	90	49.5	30.5	171.7	25.0	255.1	74.9	68.4	675.1	503.4
91_47	100	55.5	42.4	190.0	29.0	301.7	81.4	78.7	778.6	588.6
91_48	92	48.6	40.8	165.1	25.4	250.9	66.3	70.3	667.3	502.3
91_49	89	49.5	47.8	167.0	29.1	275.2	83.9	75.0	727.5	560.5
91_50	96	49.8	47.8	168.0	31.1	263.9	85.1	75.1	720.6	552.7
91_51	85	50.7	41.0	172.6	28.4	247.0	74.4	73.9	688.0	515.4
91_52	85	47.5	32.5	163.8	26.5	191.8	57.3	65.4	584.9	421.1
91_53	23	3.6	3.1	12.7	3.1	0.0	0.0	4.5	26.9	14.2
92_01	43	8.7	5.7	31.1	5.6	15.4	4.4	10.0	80.9	49.8
92_02	85	56.0	44.2	191.6	28.0	247.1	63.2	79.7	709.9	518.3
92_03	95	65.8	58.9	222.7	32.9	395.5	97.7	97.5	971.0	748.4
92_04	100	57.2	56.1	192.5	27.4	300.8	72.9	86.8	793.7	601.2
92_05	100	55.1	54.2	186.0	29.9	260.5	72.3	82.6	740.5	554.5
92_06	100	51.2	45.6	173.9	29.5	169.4	55.5	74.3	599.3	425.4
92_07	103	66.1	53.3	226.5	32.4	340.4	89.3	94.3	902.4	675.9
92_08	99	61.0	47.5	210.8	30.3	325.3	91.1	83.7	849.7	638.8
92_09	104	65.5	54.1	224.8	31.4	366.1	93.2	92.2	927.2	702.5
92_10	103	75.8	69.2	256.6	34.9	456.1	105.9	113.0	1111.4	854.9
92_11	103	68.3	67.4	230.3	33.0	325.0	79.4	102.8	906.2	675.9
92_12	99	60.7	65.9	205.3	29.8	225.5	57.4	90.3	734.9	529.6
92_13	103	60.9	57.2	206.5	29.4	320.9	79.2	91.1	845.2	638.7
92_14	101	69.1	54.4	236.2	31.9	413.7	101.9	99.5	1006.7	770.5
92_15	103	79.0	52.3	230.5	31.1	398.4	97.7	96.5	985.4	754.9
92_16	100	63.0	43.1	186.9	24.8	303.6	74.9	76.4	772.7	585.8
92_17	101	62.8	55.5	213.8	31.5	348.9	91.7	91.0	895.2	681.4
92_18	96	62.8	61.3	212.3	30.7	386.3	94.7	95.0	943.1	730.8
92_19	99	55.0	57.5	185.7	27.4	332.8	84.7	82.6	825.6	639.9
92_20	100	55.6	56.6	188.1	27.1	335.4	81.5	83.7	828.0	639.9
92_21	104	56.7	47.6	192.7	27.0	333.8	82.0	83.6	823.4	630.7
92_22	105	63.8	50.2	218.0	30.0	385.3	94.2	92.7	934.2	716.3
92_23	100	58.4	51.1	200.9	28.7	321.7	81.2	81.2	823.2	622.3
92_24	99	69.0	63.4	234.5	36.0	406.5	105.7	101.1	1016.2	781.7
92_25	104	49.4	42.5	208.2	26.7	357.3	85.4	86.8	856.3	648.1
92_26	96	56.6	58.5	192.0	34.2	311.8	102.2	84.1	839.4	647.4

92_27	94	51.1	52.2	173.3	26.3	291.3	79.2	76.1	749.5	576.2
92_28	93	49.7	45.5	168.9	28.1	268.3	83.8	72.8	717.2	548.3
92_29	103	59.2	45.6	202.5	32.1	328.3	100.6	84.1	852.5	650.0
92_30	97	58.5	46.8	201.3	25.5	334.1	81.5	81.6	829.3	628.0
92_31	90	46.7	38.6	158.9	22.5	266.6	63.8	67.6	664.5	505.7
92_32	100	59.6	55.4	201.4	30.1	331.2	84.0	89.4	851.1	649.7
92_33	97	57.6	57.5	194.2	29.4	356.3	90.4	87.3	872.6	678.5
92_34	100	55.4	56.7	187.0	35.4	292.9	94.2	83.1	804.7	617.7
92_35	101	62.6	57.4	211.5	31.5	375.3	95.0	93.2	926.6	715.1
92_36	97	66.6	55.7	226.2	32.7	400.7	102.1	97.3	981.4	755.1
92_37	104	66.3	51.9	227.5	46.7	313.0	124.5	93.2	923.2	695.7
92_38	95	50.2	37.7	172.8	26.2	265.9	77.4	70.2	700.4	527.7
92_39	100	53.4	38.3	181.4	26.2	312.9	78.9	78.2	769.3	587.9
92_40	99	58.0	48.6	195.5	32.9	337.6	90.0	87.4	849.9	654.5
92_41	97	61.3	63.0	206.7	33.0	345.0	91.7	92.1	892.7	686.0
92_42	100	52.1	50.3	175.5	27.4	304.3	80.0	77.7	767.2	591.8
92_43	100	57.3	47.4	194.1	29.0	336.2	88.8	83.2	835.9	641.8
92_44	102	57.3	42.1	197.0	37.9	258.7	84.5	80.1	757.6	560.7
92_45	103	70.7	55.6	243.2	39.9	370.0	113.0	99.5	991.9	748.7
92_46	103	72.8	64.1	247.0	35.2	419.7	102.6	107.2	1048.6	801.6
92_47	102	59.4	54.9	201.0	29.7	308.1	70.1	88.6	811.8	610.8
92_48	100	61.4	61.0	207.1	35.5	329.8	98.8	93.3	886.9	679.8
92_49	101	59.3	57.4	200.2	30.2	356.6	94.8	89.7	888.3	688.0
92_50	97	56.9	48.2	193.9	27.4	338.7	87.0	83.4	835.4	641.5
92_51	102	60.3	42.9	207.3	27.3	340.1	86.6	83.8	848.4	641.1
92_52	104	66.3	48.7	229.3	27.3	369.6	83.5	90.3	915.1	685.7
92_53	58	18.0	14.9	62.2	8.7	95.5	26.4	24.8	250.4	188.2
93_01	24	1.8	1.3	6.7	0.9	4.7	2.9	1.6	20.0	13.3
93_02	101	45.6	39.6	155.6	20.2	256.7	61.5	65.5	644.6	489.0
93_03	99	51.8	52.0	174.7	26.9	304.1	82.2	78.4	770.2	595.4
93_04	102	54.9	53.7	185.4	27.3	340.5	84.8	82.7	829.3	643.9
93_05	103	60.3	50.2	204.6	27.6	374.4	88.9	88.0	894.0	689.3
93_06	105	73.4	55.3	251.5	38.1	426.0	120.5	105.0	1069.8	818.3
93_07	102	67.8	52.2	233.5	35.9	378.4	115.0	94.2	977.0	743.5
93_08	102	62.7	51.8	214.1	33.6	351.9	103.5	90.2	907.8	693.6
93_09	102	69.3	61.7	234.2	34.8	422.3	105.4	103.3	1030.9	796.7
93_10	100	63.3	62.6	213.4	37.2	368.7	110.6	96.1	951.7	738.4
93_11	99	62.5	62.7	210.9	34.3	380.9	110.5	94.8	956.5	745.7
93_12	103	56.1	52.4	189.8	31.5	324.3	98.4	83.1	835.7	645.9
93_13	100	56.6	39.8	193.0	29.5	319.8	90.7	81.8	811.1	618.1
93_14	104	49.5	35.2	171.1	23.2	268.1	70.2	67.5	685.0	513.8
93_15	100	65.8	53.9	224.8	35.6	371.0	106.2	94.4	951.6	726.8
93_16	102	62.5	55.5	212.1	29.5	385.5	90.4	92.1	927.7	715.6
93_17	101	63.7	62.4	214.9	31.6	404.0	103.9	96.5	976.9	762.0
93_18	102	63.2	66.0	213.4	29.7	404.7	92.7	95.8	965.5	752.1
93_19	103	57.8	55.9	195.4	28.7	340.4	94.8	86.8	859.8	664.4
93_20	105	73.1	60.9	248.3	36.4	421.0	110.9	107.7	1058.4	810.1
93_21	101	66.0	47.9	227.2	28.9	370.0	101.3	94.5	935.9	708.7
93_22	102	61.3	52.0	209.9	30.2	360.5	92.9	87.2	894.0	684.0
93_23	99	61.4	54.0	208.4	29.8	367.6	97.3	91.2	909.7	701.3
93_24	105	61.8	60.5	208.5	34.3	348.9	134.9	93.3	942.2	733.7
93_25	102	57.1	59.5	193.2	28.1	332.1	96.1	86.3	852.3	659.1
93_26	102	46.9	46.0	159.0	26.3	223.1	104.7	70.0	675.9	516.9
93_27	101	62.7	52.6	212.5	31.9	329.6	140.7	92.9	922.8	710.4

93_28	104	65.1	46.5	222.3	31.3	386.2	100.1	92.8	944.3	722.0
93_29	103	54.5	43.2	186.6	24.6	320.5	76.9	76.4	782.7	596.1
93_30	99	56.3	48.7	190.8	27.6	347.2	83.4	83.0	836.9	646.1
93_31	102	62.2	59.7	209.6	30.8	394.1	94.8	93.8	945.0	735.4
93_32	101	61.1	90.9	208.2	27.7	361.6	89.3	86.2	925.0	716.8
93_33	104	56.9	57.5	191.9	27.5	344.9	92.5	85.5	856.7	664.8
93_34	105	66.9	60.3	226.3	33.3	398.0	92.7	99.7	977.4	751.0
93_35	102	68.9	52.5	234.7	30.6	425.6	97.6	100.4	1010.3	775.6
93_36	89	52.5	43.0	179.9	25.1	300.7	69.8	74.7	745.7	565.8
93_37	80	48.8	41.0	167.0	22.5	284.3	63.6	69.8	697.0	530.0
93_38	104	64.1	59.2	217.2	29.9	389.0	88.2	94.7	942.2	725.1
93_39	102	64.6	65.5	218.1	30.4	404.8	91.8	97.7	972.9	754.8
93_40	102	66.1	67.7	223.0	36.4	380.9	107.0	99.6	980.7	757.6
93_41	102	67.6	61.0	228.5	35.6	395.1	106.5	100.9	995.2	766.7
93_42	99	64.4	46.5	220.7	29.0	384.6	88.7	92.4	926.3	705.6
93_43	102	64.3	48.7	221.7	29.5	358.2	82.0	89.5	893.9	672.2
93_44	104	63.9	51.5	219.4	28.6	345.5	81.9	89.6	880.3	660.9
93_45	104	71.4	63.4	242.7	32.9	393.8	89.5	104.4	998.1	755.4
93_46	102	67.2	34.8	227.2	35.2	399.4	106.9	101.1	971.9	744.7
93_47	103	68.6	54.3	231.5	35.2	415.2	98.9	104.3	1007.9	776.4
93_48	76	36.7	36.3	124.0	17.2	205.0	44.5	54.8	518.6	394.5
93_49	79	50.9	38.4	174.4	23.3	273.6	84.3	72.2	717.1	542.7
93_50	91	41.2	26.7	142.5	20.2	210.4	59.2	55.6	555.9	413.3
93_51	102	65.9	50.7	226.9	30.7	367.2	87.8	92.4	921.7	694.7
93_52	99	57.9	49.9	197.3	32.4	317.2	93.8	84.2	832.7	635.5
Total		6795.	5881.	23103.	3451.	37674.	10261.	9854.	97018.	73915.
W.Avg		56.	49.	191.	29.	311.	85.	81.	802.	611.
FY91 Tot		76.	40.	258.	42.	118.	178.	80.	793.	535.
FY92 Tot		2821.	2446.	9586.	1457.	15064.	4103.	4076.	39552.	29966.
FY93 Tot		3112.	2765.	10579.	1565.	18046.	4850.	4557.	45473.	34894.
FY94 Tot*		786.	630.	2680.	386.	4446.	1131.	1141.	11200.	8520.
CY91 Tot		606.	473.	2079.	345.	2662.	985.	829.	7980.	5901.
CY92 Tot		3102.	2712.	10525.	1576.	17030.	4492.	4508.	43945.	33419.
CY93 Tot		3087.	2696.	10499.	1530.	17982.	4783.	4517.	45093.	34594.
CY94 Tot*		0.	0.	0.	0.	0.	0.	0.	0.	0.

NOTE: The "*" next to FY and CY totals means that the year is not fishished yet

F Web Version of the YAG

The **User Guide** and **Instrument Guide** of the **Yohkoh Analysis Guide (YAG)** may be viewed as **Web documents** on the URL's:

- **http://diapason.lmsal.com/~bentley/guides/yag/**
- **http://umbra.nascom.nasa.gov/~bentley/guides/yag/**
- **http://ydac.mssl.ucl.ac.uk/guides/yag/**

PostScript versions of the **User Guide** and **Instrument Guide** are available at each site - they are designed to be printed double-sided. If you want a printed copy of the **YAG**, the PostScript version is recommended since the screen representation of special characters in the Hypertext version does not produce good printed output.

This version of the **YAG** was prepared at the **YDAC** (located at the Mullard Space Science Laboratory, University College London) by **Bob Bentley**. The Hypertext version was translated from LaTeX using **TtH**, and further formatted using **IDL**.